

Ultrapotent Broadly Neutralizing Human-llama Bispecific Antibodies against HIV-1

Jianliang Xu,* Tongqing Zhou, Krisha McKee, Baoshan Zhang, Cuiping Liu, Alexandra F. Nazzari, Amarendra Pegu, Chen-Hsiang Shen, Jordan E. Becker, Michael F. Bender, Payton Chan, Anita Changela, Ridhi Chaudhary, Xuejun Chen, Tal Einav, Young Do Kwon, Bob C. Lin, Mark K. Louder, Jonah S. Merriam, Nicholas C. Morano, Sijy O'Dell, Adam S. Olia, Reda Rawi, Ryan S. Roark, Tyler Stephens, I-Ting Teng, Emily Tourtellott-Fogt, Shuishu Wang, Eun Sung Yang, Lawrence Shapiro, Yaroslav Tsybovsky, Nicole A. Doria-Rose, Rafael Casellas, and Peter D. Kwong*

Broadly neutralizing antibodies are proposed as therapeutic and prophylactic agents against HIV-1, but their potency and breadth are less than optimal. This study describes the immunization of a llama with the prefusion-stabilized HIV-1 envelope (Env) trimer, BG505 DS-SOSIP, and the identification and improvement of potent neutralizing nanobodies recognizing the CD4-binding site (CD4bs) of vulnerability. Two of the vaccine-elicited CD4bs-targeting nanobodies, G36 and R27, when engineered into a triple tandem format with llama IgG2a-hinge region and human IgG1-constant region (G36×3-IgG2a and R27×3-IgG2a), neutralized 96% of a multiclade 208-strain panel at geometric mean IC_{80s} of 0.314 and 0.033 μg mL⁻¹, respectively. Cryo-EM structures of these nanobodies in complex with Env trimer revealed the two nanobodies to neutralize HIV-1 by mimicking the recognition of the CD4 receptor. To enhance their neutralizing potency and breadth, nanobodies are linked to the light chain of the V2-apex-targeting broadly neutralizing antibody, CAP256V2LS. The resultant human-llama bispecific antibody CAP256L-R27×3LS exhibited ultrapotent neutralization and breadth exceeding other published HIV-1 broadly neutralizing antibodies, with pharmacokinetics determined in FcRn-Fc mice similar to the parent CAP256V2LS. Vaccine-elicited llama nanobodies, when combined with V2-apex broadly neutralizing antibodies, may therefore be able to fulfill anti-HIV-1 therapeutic and prophylactic clinical goals.

retain full antigen specificity with a single antibody domain.^[2] They can penetrate tissues and recognize epitopes that are often inaccessible to conventional antibodies.^[2] Such “hidden” epitopes also have the potential to be conserved across viral strains, making nanobodies ideal antiviral molecules with great cross-reactivity to multiple viral pathogens. HIV-1 broadly neutralizing antibodies (bNAbs) target vulnerable epitopes on the envelope (Env) trimer, such as the CD4-binding site (CD4bs), V2-apex, V3-glycan, and fusion peptide (FP).^[3] However, it usually takes years for bNAbs to develop as they need to overcome extensive barriers to acquire the ability to target epitopes beneath the Env glycan shield.^[4] In contrast, nanobodies may be able to overcome such barriers more easily by virtue of their extended CDR3s and single domain character, which enables them to access Env crevices. Indeed, a broad and potent nanobody J3 has been identified from gp140 immunization in llama and shown to mimic CD4 binding.^[5] Recently, in a proof of concept study, we created a bispecific antibody that fuses J3 to the light chain of the potent

1. Introduction

Nanobodies are antigen-binding entities typically derived from the heavy chain-only antibodies of camelid animals,^[1] and they

 The ORCID identification number(s) for the author(s) of this article can be found under <https://doi.org/10.1002/adv.202309268>

© 2024 The Authors. Advanced Science published by Wiley-VCH GmbH. This article has been contributed to by U.S. Government employees and their work is in the public domain in the USA. This is an open access article under the terms of the [Creative Commons Attribution](#) License, which permits use, distribution and reproduction in any medium, provided the original work is properly cited.

DOI: 10.1002/adv.202309268

J. Xu, T. Zhou, K. McKee, B. Zhang, C. Liu, A. F. Nazzari, A. Pegu, C.-H. Shen, M. F. Bender, A. Changela, R. Chaudhary, X. Chen, Y. D. Kwon, B. C. Lin, M. K. Louder, J. S. Merriam, S. O'Dell, A. S. Olia, R. Rawi, I-T. Teng, E. Tourtellott-Fogt, S. Wang, E. S. Yang, N. A. Doria-Rose, P. D. Kwong
Vaccine Research Center
National Institute of Allergy and Infectious Diseases
National Institutes of Health
Bethesda, MD 20892, USA
E-mail: jxu40@gsu.edu; pdkwong@nih.gov

V2-apex antibody CAP256V2LS and observed synergistic neutralization between J3 and CAP256V2LS, with substantially improved breadth and potency.^[6] Several other bispecific and trispecific antibodies have also been reported, such as VRC01-PGDM1400-10E8v4,^[7] N6-PGDM1400-10E8v4,^[7] and Tri-Nab,^[8] which achieve near pan neutralization of a 208-strain panel with geometric mean IC₅₀s of $\approx 0.15 \mu\text{g mL}^{-1}$.

We have previously designed an HIV-1 Env trimer BG505 DS-SOSIP, a highly desirable antigen that is conformationally fixed in a prefusion-closed state, in which neutralizing epitopes are almost exclusively exposed and non-neutralizing or poorly neutralizing epitopes are hidden, even in the presence of CD4.^[9] In a recent clinical trial evaluating its safety and immunogenicity, we found that three injections of BG505 DS-SOSIP elicited binding antibodies against trimer immunogen in all groups, however, most of these antibodies targeted the glycan-free trimer base.^[10] From one donor, by sorting B cells that can bind to glycan-base covered BG505 trimer, we identified autologous neutralizing antibodies against the fusion-peptide site of vulnerability.^[11] In this study, we explore the ability of BG505 DS-SOSIP to elicit a neutralizing response in llama by repetitive immunizations and isolate broadly neutralizing nanobodies using Env trimer and subdomains of trimer. We further explore generalizable strategies for nanobody improvement and combine the most potent nanobodies with CAP256V2LS to create ultrapotent human-llama bispecific antibodies against HIV-1.

J. Xu, R. Casellas
Laboratory of Lymphocyte Nuclear Biology
National Institute of Arthritis and Musculoskeletal and Skin Diseases
NIH
Bethesda, MD 20892, USA

J. Xu, P. Chan
Department of Biology
Georgia State University
Atlanta, GA 30303, USA

J. E. Becker, N. C. Morano, R. S. Roark, L. Shapiro
Zuckerman Mind Brain Behavior Institute
Columbia University
New York, NY 10027, USA

J. E. Becker, N. C. Morano, R. S. Roark, L. Shapiro
Department of Biochemistry and Molecular Biophysics
Columbia University Vagelos College of Physicians and Surgeons
New York, NY 10032, USA

T. Einav
Center for Vaccine Innovation
La Jolla Institute for Immunology
La Jolla, CA 92037, USA

T. Stephens, Y. Tsybovsky
Electron Microscopy Laboratory
Cancer Research Technology Program
Leidos Biomedical Research
Frederick National Laboratory for Cancer Research
Frederick, MD 21702, USA

L. Shapiro, P. D. Kwong
Aaron Diamond AIDS Research Center
Columbia University Vagelos College of Physicians and Surgeons
New York, NY 10032, USA

R. Casellas
Hematopoietic Biology and Malignancy
MD Anderson Cancer Center
Houston, TX 77054, USA

2. Results

2.1. BG505 DS-SOSIP Immunized Llama Develops Broadly Neutralizing Serum Responses

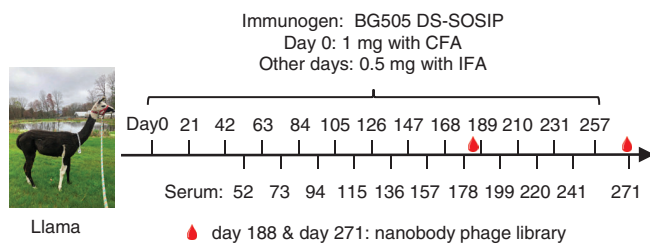
To explore the anti-HIV potential of nanobodies, we immunized a llama with prefusion-stabilized HIV-1 Env trimer BG505 DS-SOSIP and sought to isolate broadly HIV-1 neutralizing nanobodies. We immunized the llama 13 times (Figure 1A) and monitored the serum antibody response against multiple HIV Env probes over the course of 271 days (Figure 1B). The immunization quickly induced strong autologous sera titer, as well as slightly weaker titer against BG505 (CD4bs KO 4115), the CD4bs epitope knocked out version of BG505 DS-SOSIP, indicating the existence of CD4bs directed response on BG505 DS-SOSIP. The antibody responses were weaker against glycan base-covered Env trimer BG505 DS-SOSIP (4mut N502-660) at early time points, suggesting that the early immune response was primarily directed against the exposed base region of the soluble HIV-1 Env trimer. This result aligns well with the almost exclusive glycan-free trimer base-targeting antibody responses observed in the 3-dose clinical trial study. However, starting from day ≈ 115 , a stronger response developed against the glycan-base covered Env trimer and Env of ConC strain, suggestive of non-base epitope targeting and cross-clade recognition. Interestingly, epitope-specific antibody responses against the CD4bs-specific probe RSC3^[31] and the fusion peptide-specific probe FP8^[12] were not detected until later time points in the immunization.

Consistent with ELISA results at days 52, 73, and 94 showing an early response primarily focused on the Env trimer base, the serum neutralizing potency and breadth on a 14-strain panel were weak at these three time points, and the serum neutralization response improved substantially starting on day 115 (Figure 1C). The neutralization breadth reached 100% by day 178, and the potency against the tested 14 strains continued to increase until the termination of the experiment on day 271. We further tested the neutralization activity of the sera from days 178 and 271 on an unbiased 50-strain panel.^[13] The data on the non-overlapping 60-strains from the two panels showed that the neutralization breadth increased from 77% on day 178 to 88% by day 271, and the neutralization titer (geometric mean ID₅₀) increased from 357 on day 178 to 1032 on day 271 (Figure 1D; Figure S1A, Supporting Information). Neutralization fingerprinting analysis^[14] predicted that the majority of the neutralization was VRC01-like (66%–70%), indicating that CD4bs-directed antibody response was dominant (Figure S1B, Supporting Information). These results demonstrated that BG505 DS-SOSIP can elicit a broad and potent anti-HIV-1 antibody response in llama within a short period of time.

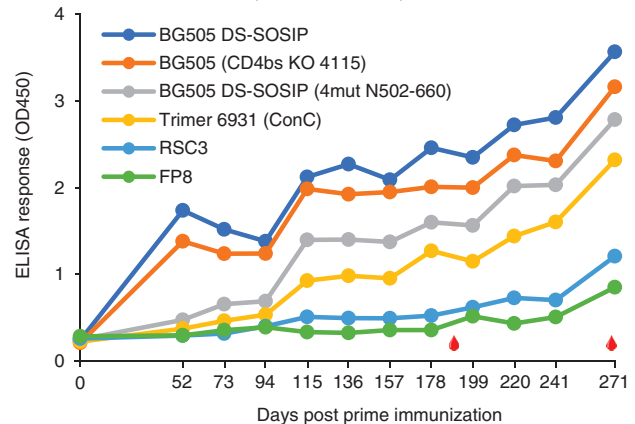
2.2. Isolation of HIV-1 Neutralizing Nanobodies

To isolate monoclonal neutralizing nanobodies, we constructed a nanobody phage library from the PBMCs of the llama on day 188, which is 10 days after serum neutralizing breadth first reached 100% on a 14-strain panel (Figure 2A). Four protein/peptide probes were used for nanobody screening: Env Trimer (BG505 DS-SOSIP), Fusion peptide, Glycan-base trimer (BG505 DS-SOSIP.4mut_N502-660), and RSC3. The nanobodies identified

A Llama immunization scheme



B Llama sera ELISA (10000x dilution)



C 14-strain panel neutralization of llama sera (ID₅₀)

Tier	Clade	Virus	day 0	day 52	day 73	day 94	day 115	day 136	day 157	day 178	day 199	day 220	day 241	day 271	
N/A	A	BG505.W6M.C2.T332N.SG3	<20	85	269	324	2,077	4,173	1,918	4,992	6,655	11,077	10,997	16,116	
1B	A	Q23.17.SG3	<20	<20	<20	<20	746	1,566	851	1,770	3,055	4,060	3,929	10,600	
2	A	RW020.2.SG3	<20	<20	<20	22	556	1,044	353	661	1,341	1,506	1,292	3,971	
2	AC	3301.v1.c24.SG3	<20	<20	<20	<20	43	112	50	151	276	319	394	1,181	
2	AD	Q168.a2.SG3	<20	<20	<20	<20	122	186	269	857	1,771	2,555	2,478	5,176	
2	B	JRCSF.JB.SG3	<20	<20	77	158	777	2,060	1,438	2,007	2,578	2,840	3,819	5,384	
2	B	QH0515.01.SG3	<20	<20	<20	<20	64	107	59	301	777	836	1,457	3,363	
2	B	RHPA.7.SG3	<20	<20	<20	<20	39	110	91	459	831	969	1,114	3,170	
2	B	TRO.11.SG3	<20	<20	<20	<20	86	181	39	274	656	628	736	2,239	10,000-100,000
N/A	C	CAP256.206.C9.SG3	<20	<20	<20	<20	<20	28	20	96	176	177	224	500	1,000-10,000
1A	C	MW965.26.SG3	<20	37	236	135	1,183	2,396	1,151	5,578	6,132	7,799	7,704	21,896	100-1,000
2	C	ZM233.6.SG3	<20	<20	<20	<20	<20	56	35	136	218	250	333	544	100-1,000
2	C	ZM249.1.SG3	<20	<20	<20	<20	<20	<20	<20	86	208	174	123	427	100-1,000
N/A	D	NKU3006.ec1.SG3	<20	<20	76	72	489	1,489	710	1,231	1,893	2,265	2,404	5,044	10-100
non-HIV		SIVmac251.30.SG3	<20	<20	<20	<20	<20	<20	<20	<20	<20	<20	<20	<20	

D 60-strain panel neutralization of llama sera (ID₅₀)

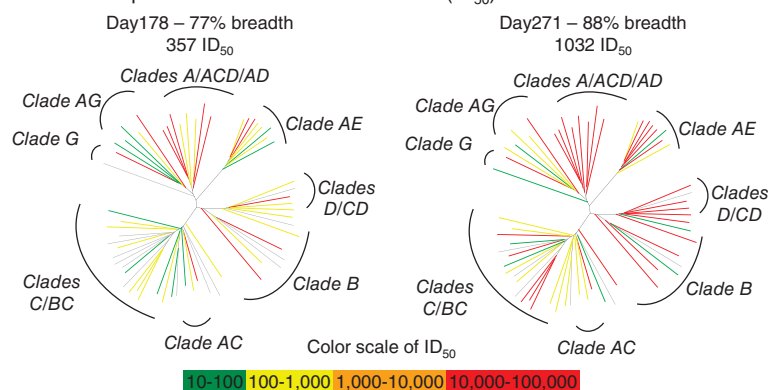
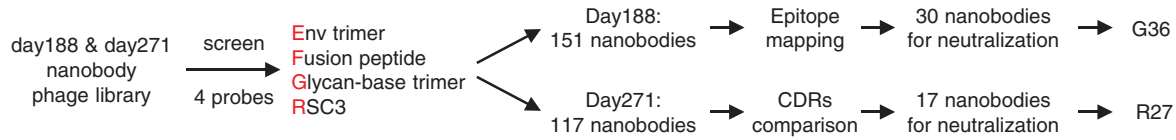


Figure 1. BG505 DS-SOSIP immunized llama develops broadly neutralizing serum responses. A) Immunization schema in a llama. The llama was immunized with BG505 DS-SOSIP subcutaneously once every 21 days (except the last boost) as indicated above the arrow line, and serum was collected 10 days post each immunization starting from day 52 as indicated beneath the arrow line. B) Antibody binding response to HIV Env probes in the immunized llama as determined by ELISA. C) Llama sera neutralization response on a 14-strain panel. Color shading represents potency as indicated on the right of the table. D) Dendrograms of the neutralization activity of day 188 and day 271 sera on a 60-strain panel. Dendrograms display the diversity of tested viral strains, with branches colored according to neutralization potency (non-neutralized branches shown in gray).

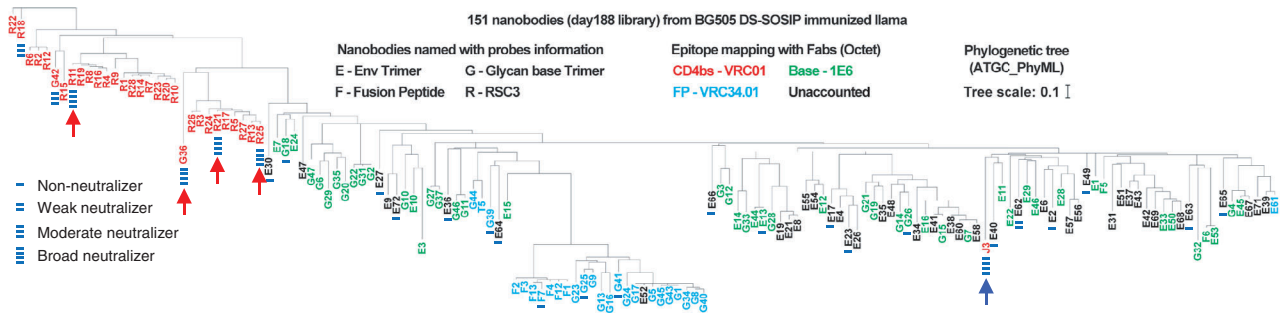
using these probes were named after the first letter of each corresponding probe name (underlined in the probe name) followed by a number. In total, 151 nanobodies with unique sequences were identified and expressed for further analysis. The binding epitopes on HIV-1 Env for these nanobodies were mapped by

a competition Biolayer interferometry (BLI) assay using Fabs of five antibodies with known epitopes: VRC01^[31] for the CD4bs, VRC34.01^[3e] for the FP epitope, 1E6 (also called RM19R)^[15] for the Env-base, PGT145^[16] for the V2-apex, and 10-1074^[17] for the V3 glycan (Figure S2A,B, Supporting Information). Of the

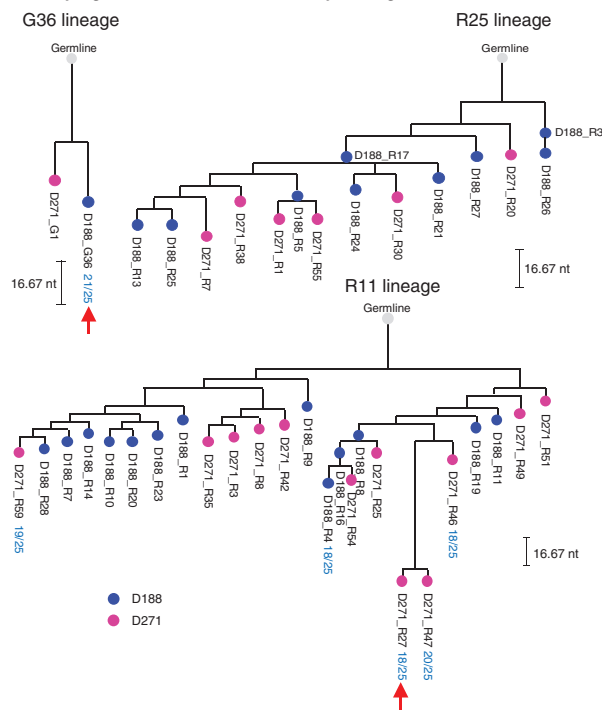
A Nanobody screening strategy



B Phylogenetic tree of day 188 nanobodies with epitope mapping classification



C Phylogenetic tree of 3 nanobody lineages



D 25-strain neutralization of top 6 nanobodies (IC₅₀ µg/mL)

clade	Virus	D188_ R4	D188_ G36	D271_ R27	D271_ R46	D271_ R47	D271_ R59	J3
A	BG505.W6M.C2.T332N.SG3	0.003	0.003	0.0008	0.002	0.001	0.001	0.463
A	Q23.17.SG3	0.016	0.0008	0.005	0.009	0.003	0.003	4.69
A	3415.v1.c1.SG3	>10	0.083	>10	>10	6.060	>10	0.082
A	BB539.2B13.SG3	0.175	0.020	0.085	0.086	0.057	0.071	0.282
A	BG505.W6M.C2.SG3	0.011	0.012	0.005	0.006	0.004	0.007	4.06
A	BI369.9A.SG3	0.303	0.036	0.076	0.135	0.018	0.036	0.475
AE	C1080.c3.SG3	3.400	0.579	2.750	1.600	1.920	1.440	0.744
AE	C2101.c1.SG3	0.015	0.075	0.008	0.006	0.008	0.006	4.08
AE	C4118.09.SG3	0.070	0.050	0.044	0.025	0.065	0.023	7.01
AE	CNE56.SG3	0.586	0.031	0.487	0.289	0.741	1.530	1.18
AG	269-12.SG3	>10	6.320	>10	>10	>10	>10	0.144
AG	T266-60.SG3	0.122	>10	0.047	0.017	0.031	0.084	1.42
B	JRC5F.JB.SG3	0.786	0.003	0.317	0.740	0.072	0.103	0.119
B	QH0515.01.SG3	0.055	0.027	0.049	0.047	0.052	0.033	0.351
BC	CNE7.SG3	0.140	7.940	0.020	0.042	0.073	0.064	0.056
C	CAP256.206.C9.SG3	3.760	0.291	0.635	3.520	0.343	0.257	0.596
C	ZM233.6.SG3	2.300	0.052	1.320	1.380	1.510	1.720	4.1
C	0077.v1.c16.SG3	>10	7.360	>10	>10	>10	>10	0.266
C	CAP210.E8.SG3	>10	7.790	>10	>10	>10	>10	0.26
C	CAP45.G3.SG3	3.130	>10	1.540	1.360	1.740	2.980	>10
C	CNE30.SG3	4.330	>10	2.300	2.420	6.810	2.100	0.093
C	CNE31.SG3	>10	0.269	>10	>10	>10	>10	0.043
C	DUI56.12.SG3	>10	1.240	>10	>10	8.420	7.070	0.344
D	6405.v4.c34.SG3	>10	>10	>10	>10	>10	>10	7.21
D	A03349M1.vrc4a.SG3	1.250	1.500	0.420	0.480	0.541	0.593	2.6
	# Viruses	25	25	25	25	25	25	25
	Neutralized IC50 <50 µg/mL	18	21	18	18	20	19	24
	Geometric Mean IC50	0.239	0.129	0.101	0.117	0.143	0.121	0.602
			<0.001	0.001-0.01	0.01-0.1	0.1-1	1-10	

Figure 2. Identification of neutralizing nanobodies from BG505 DS-SOSIP immunized llama. A) Nanobody phage library construction and screening. The four probes used for phage screening are: Env Trimer (BG505 DS-SOSIP), Fusion peptide (BG505 DS-SOSIP.4mut_N502-660), and RSC3. B) Summary of epitopes of 151 nanobodies from day 188 library. 30 nanobodies selected for small panel neutralization test are grouped into 4 categories: Non-neutralizer (one line); Weak neutralizer (two lines); Moderate neutralizer (three lines); Broad neutralizer (four lines plus one red arrow). Control nanobody J3 is marked with four lines and one blue arrow. C) Phylogenetic tree of three selected nanobody lineages. 42 nanobodies from the three lineages were tested on a 10-strain panel first, then the top 6 candidates were further tested on an additional 15-strain panel. Neutralization breadth of the top 6 nanobodies on a 25-strain panel is shown beneath the nanobody names. Scale bars indicate the distance of 16.67 nucleotides (nt) in each tree. D) 25-strain neutralization of the top 6 nanobodies from Figure S3C (Supporting Information). The broadest (G36) and most potent (R27) nanobodies were selected for further analysis.

69 nanobodies identified by the Env trimer probe, 4 competed with VRC34.01, 19 competed with 1E6, and 46 did not compete with any of the five antibodies. Of the 9 nanobodies identified with the FP probe, 7 competed with VRC34.01, and 2 competed with 1E6. Of the 45 nanobodies identified with the Glycan-base

trimer, 12 competed with VRC01, 17 competed with VRC34.01, and 26 competed with 1E6. Interestingly, all 28 nanobodies identified with the RSC3 probe competed with VRC01, indicating that these nanobodies are CD4bs-targeting. More importantly, phylogenetic analysis of the 151 Env-binding nanobodies

showed that VRC01-competing nanobodies and VRC34.01-competing nanobodies formed two distinct clusters (Figure 2B). Based on the phylogenetic tree, we selected 30 representative nanobodies, 10 VRC34.01- or 1E6-competing, 14 non-competing, and 6 VRC01-competing, and tested their neutralization activity on the same 14-strain panel used for the initial serum test. None of the 10 VRC34.01- or 1E6-competing nanobodies neutralized any strain (non-neutralizers). Only 1 of the 14 non-competing nanobodies neutralized 2 strains (weak neutralizers) (Figure 2B; Figure S2C, Supporting Information). However, the 6 VRC01-competing nanobodies neutralized these 14 strains, with various potency and breadth (Figure S2D, Supporting Information). Specifically, we identified 4 broad neutralizers. G36 neutralized all 14 strains with a geometric mean IC_{50} of $0.088 \mu\text{g mL}^{-1}$; R11, R21, and R25 neutralized over 11 strains out of 14; and two moderate neutralizers, G42 and R18, neutralized 8 strains out of 14.

We next constructed a second nanobody phage library from the day 271 PBMCs, carried out the same screening, and identified 117 new nanobodies with unique amino acid sequences. By comparing their complementarity-determining region (CDR) sequences, day 271 nanobodies that were similar to day 188 non-neutralizers or weak neutralizers were removed from further analysis. From the remaining nanobodies, 17 representative ones were selected for neutralization assessment on a 5-strain panel that included representative clades in the above-mentioned 14-strain panel (Figure S3A,B, Supporting Information). Among these 17 nanobodies, R27, E46 and G1 neutralized 5, 2, and 4 strains, respectively.

2.3. Three Lineages of HIV-1 Neutralizing Nanobodies

To obtain a more comprehensive analysis of potentially potent and broadly neutralizing nanobodies, we plotted phylogenetic trees for 42 nanobodies identified from the day 188 and day 271 libraries. These nanobodies belong to the same lineages of the 4 broad neutralizers identified from the day 188 library, namely G36, R11, R21, and R25 (Figure 2C). The D188_G36 and D271_G1 nanobodies formed a small lineage; the R11 lineage included 13 nanobodies isolated from day 188 library and 12 nanobodies from day 271 library, including D271_R27; the R21 and R25 belonged to the same lineage along with 7 other nanobodies from day 188 and 6 nanobodies from day 271. These 42 nanobodies showed diverse neutralizing breadth and potency on a 10-strain panel, and 6 of them showed 90% breadth (Figure S3C, Supporting Information); these 6 nanobodies were tested on an additional 15-strain panel. The broadest neutralizing nanobody D188_G36 (21/25, hereafter referred to as G36) and the most potent neutralizing nanobody D271_R27 (geometric mean IC_{50} : $0.101 \mu\text{g mL}^{-1}$, hereafter referred to as R27) were selected for further characterization (Figure 2D). Of note, G36 and R27 are 5–6 fold more potent in neutralizing the multiclade 25-strain panel than the previously reported nanobody J3.

2.4. Improved Neutralization Potency and Breadth by Fc Conjugation and Multimerization

As multimerization and Fc conjugation can increase the apparent affinity of nanobodies and their neutralization potency,^[18] we first

carried out such engineering for G36 and R27. A 5-strain panel test revealed that the potency of both nanobodies was improved by Fc conjugation (bivalent) based on the molarity of the whole molecules and was further improved by combining tandem multimerization and Fc conjugation (nanobody x3-IgG2a) (Figure S4A–C, Supporting Information). Of note, nanobody x3-IgG2a configuration enhanced the potency of R27 more than G36, indicating that the two nanobodies may neutralize HIV-1 via different mechanisms. Similar potency improvement patterns were seen for several other less potent and less broadly neutralizing nanobodies. Most interestingly, three VRC34.01-competing non-neutralizing nanobodies, F7, G25, and G39, became neutralizers of 1 or 3 strains after such modification, suggesting that Fc conjugation and nanobody multimerization can be a generalizable strategy for nanobody improvement (Figure S4D, Supporting Information). The improved breadth and potency of G36x3-IgG2a and R27x3-IgG2a over their monomeric (single domain) forms were further confirmed in the multiclade 25-strain panel (Figure 3A), with G36x3-IgG2a reaching 96% breadth, R27x3-IgG2a reaching 100% breadth, and both reaching higher potency than J3x3-IgG2a. The standard 208-strain panel assay was then performed on the two antibodies in x3-IgG2a format. The results showed that both nanobodies neutralized 96% of the panel at geometric mean IC_{50} s of 0.1 and $0.016 \mu\text{g mL}^{-1}$ for G36x3-IgG2a and R27x3-IgG2a, respectively (Figure 3B, with explicit IC_{50} and IC_{80} values provided in Dataset S1, Supporting Information). The breadth of 92% and 87% (with $IC_{80} < 50 \mu\text{g mL}^{-1}$) and geometric mean IC_{80} s of 0.314 and $0.033 \mu\text{g mL}^{-1}$ for G36x3-IgG2a and R27x3-IgG2a, respectively (Figure 3C; Figure S4E and Dataset S1, Supporting Information), to our knowledge, rank among the best reported HIV-1 broadly neutralizing antibodies and nanobodies.

To gain a better understanding of how the HIV-1 Env trimer interacts with nanobodies and nanobody x3-IgG2a, we performed a BLI experiment to determine the binding kinetics of BG505 DS-SOSIP to immobilized nanobody molecules, G36, R27, G36x3-IgG2a, and R27x3-IgG2a (Figure S4F, Supporting Information). By immobilizing nanobody molecules, we created multiple BG505 DS-SOSIP binding moieties on biosensors for G36 and R27, enabling comparison to G36x3-IgG2a and R27x3-IgG2a. The association and disassociation curves of all four samples could only be modeled by 1:2 (bivalent) fitting, an indication that a single BG505 DS-SOSIP molecule could indeed bind to multiple nanobody units on biosensors. The association rate of BG505 DS-SOSIP to all four molecules was similar, indicating that nanobody units of nanobody x3 versions function equally as nanobody monomers. The BG505 DS-SOSIP disassociation rate was slightly reduced in nanobody x3 format, suggesting the effect of avidity was empowered by the multiple binding units on the molecules.

2.5. Structural Basis for the Broad HIV-1 Neutralization of R27 and G36

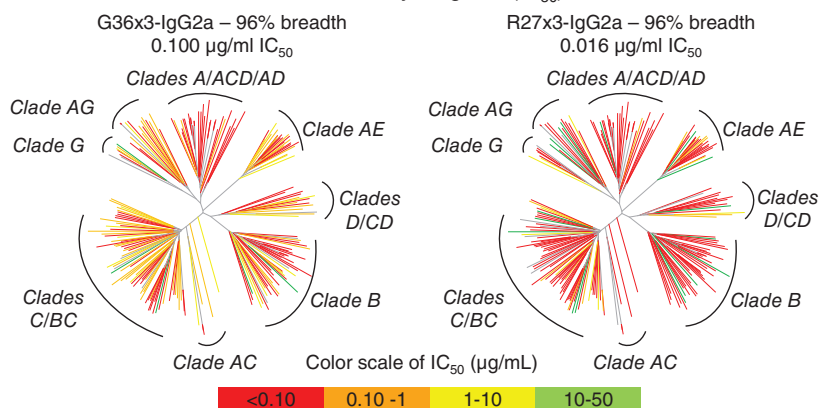
To elucidate the mechanism by which the potent and broad llama nanobodies recognized the Env trimer, we determined the structures of R27 and G36 in complex with BG505 DS-SOSIP by cryo-EM. The cryo-EM reconstruction map of R27 in complex with

A 25-strain neutralization (IC₅₀ µg/ml)

Clade	Virus	Nanobody x3-IgG2a		
		G36	R27	J3
A	BG505.W6M.C2.T332N.SG3	0.014	<0.01	0.176
A	Q23.17.SG3	0.012	<0.01	0.805
A	3415.v1.c1.SG3	0.018	0.629	0.066
A	BB539.2B13.SG3	0.122	0.006	0.490
A	BG505.W6M.C2.SG3	0.031	0.005	0.154
A	BI369.9A.SG3	0.058	0.007	0.488
AE	C1080.c3.SG3	0.641	0.029	0.309
AE	C2101.c1.SG3	0.044	0.007	1.760
AE	C4118.09.SG3	0.038	0.022	6.080
AE	CNE56.SG3	0.141	0.006	0.577
AG	269-12.SG3	0.295	6.790	0.097
AG	T266-60.SG3	3.360	0.007	1.860
B	JRCFSF.JB.SG3	0.022	<0.01	0.086
B	QH0515.01.SG3	0.032	0.007	0.185
BC	CNE7.SG3	1.870	0.014	0.026
C	CAP256.206.C9.SG3	0.350	0.072	0.503
C	ZM233.6.SG3	0.247	0.041	1.320
C	0077.v1.c16.SG3	1.880	9.870	0.182
C	CAP210.E8.SG3	3.100	1.710	0.133
C	CAP45.G3.SG3	0.181	0.019	>10
C	CNE30.SG3	0.861	0.018	0.033
C	CNE31.SG3	0.198	0.058	0.021
C	DU156.12.SG3	0.083	0.113	0.045
D	6405.v4.c34.SG3	>10	9.410	6.130
D	A03349M1.vrc4a.SG3	1.010	0.017	1.290
# Viruses		25	25	25
Neutralized IC ₅₀ <50 µg/mL		24	25	24
Geometric Mean IC ₅₀		0.165	0.056	0.295

<0.01
0.01-0.1
0.1-1
1-10

B 208-strain neutralization of nanobodyx3-IgG2a (IC₅₀)



C Llama nanobody x3-IgG2a versus other antibodies (IC₈₀)

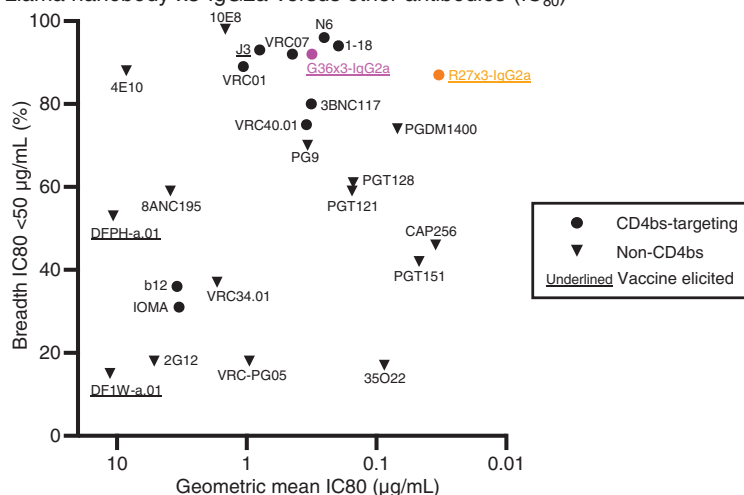
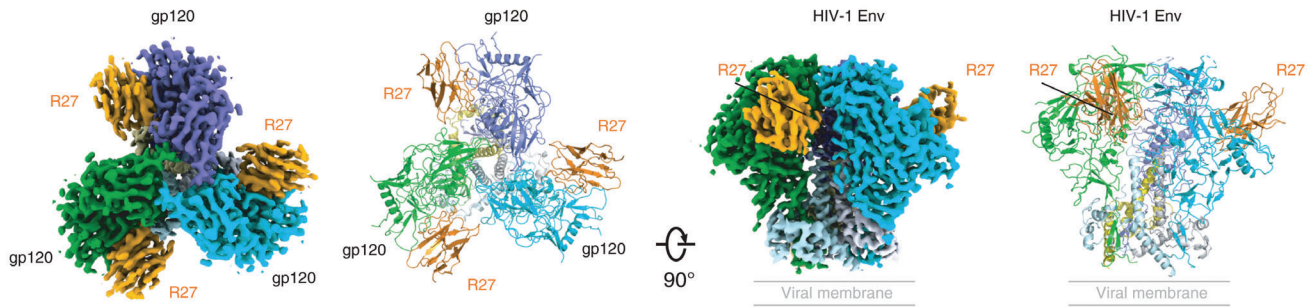


Figure 3. Immunization-elicited nanobodies, G36 and R27, in nanobody x3-IgG2a format, show broad and potent HIV-1 neutralization. A) 25-strain neutralization of nanobody x3-IgG2a. B) 208-strain panel neutralization of G36x3-IgG2a and R27x3-IgG2a. Dendrograms display the diversity of tested viral strains, with branches colored according to neutralization potency (non-neutralized branches shown in gray). IC₅₀ shown is geometric mean. C) Comparison of neutralization breadth and potency for G36x3-IgG2a and R27x3-IgG2a with other human antibodies and vaccine-elicited NHP antibodies on 208-strain panel.

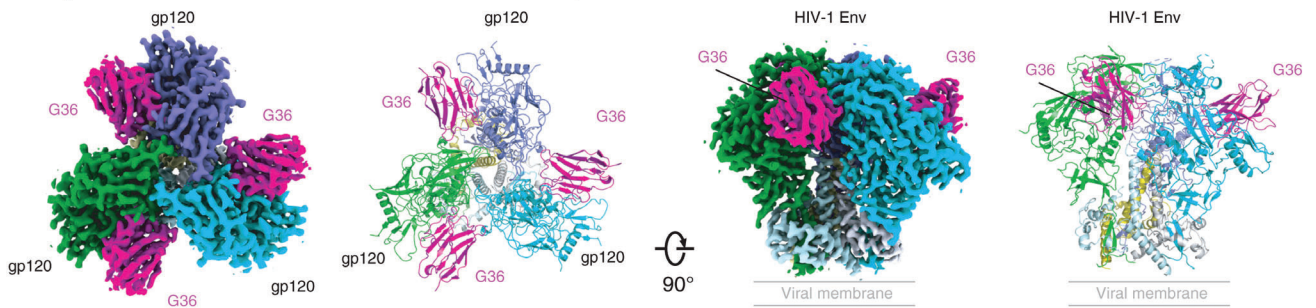
BG505 DS-SOSIP was obtained at 3.6 Å nominal resolution from 315969 particles (Figure 4A; Figure S5 and Table S1, Supporting Information). The refined structural model revealed the binding of three copies of R27, each to a protomer of the Env trimer, at the CD4bs. Cryo-EM reconstruction of G36 in complex with BG505 DS-SOSIP was achieved at 3.3 Å from 414002 particles, and the refined structure revealed a binding mode of G36 similar to that of R27 (Figure 4B; Figure S6 and Table S1, Supporting Information). The epitope of R27 covered 715 Å² on one protomer with a minor interaction of 21 Å² with a neighboring protomer (Figure 4C; Figure S7, Supporting Information). The G36 epitope was slightly larger, covering 885 Å² on one protomer and 172 Å² on the neighboring protomer (Figure 4C; Figure S8, Supporting Information). Both epitopes were at a similar location to that of J3.^[5,19] Indeed, R27, G36, and J3, as well as the domain 1 of CD4, are all bound at a similar location in the canyon between two gp120 subunits (Figure 4D). The approach angles of R27 and G36

were different (Figure 4D). This and their different sequences resulted in differences in paratope-epitope interactions between the two nanobody-Env trimer complexes. Both R27 and G36 made extensive interactions with the CD4-binding loop, loops D and V5 on the major binding gp120 protomer through residues in their CDR2 and CDR3 (Figure 4E,F; Figures S7 and S8, Supporting Information), typical for CD4bs-targeting antibodies. Moreover, G36 inserted Tyr99 into the hydrophobic “Phe43 pocket” of gp120 to mimic the CD4 Phe43-gp120 interaction (Figure 4G), similar to J3 which used Tyr99.^[19,20] Mimicry of CD4 Phe43 was also observed in the human VRC01-class antibodies, such as N6 and VRC-PG20,^[3d,21] which utilized Tyr54 or Trp54 to interact with the gp120 pocket, demonstrating the ability of immune systems to take advantage of this site of vulnerability on HIV-1 Env trimers. Overall, R27 and G36 bound at the CD4bs, in the canyon between two gp120 subunits with quaternary interactions, mimicking CD4 binding.

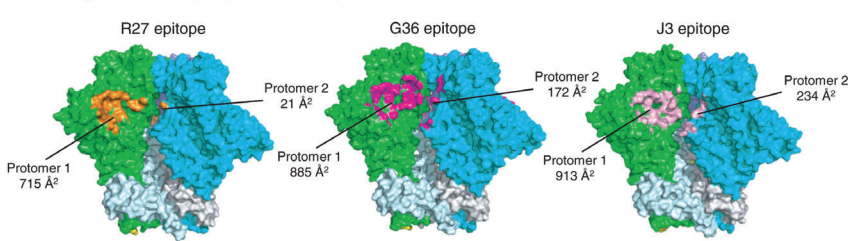
A Cryo-EM reconstruction and refined model of R27 in complex with BG505 DS-SOSIP



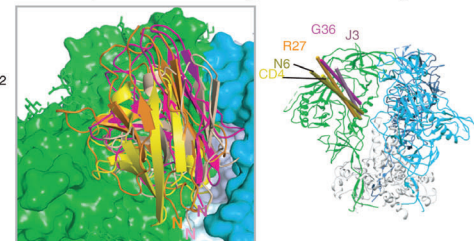
B Cryo-EM reconstruction and refined model of G36 in complex with BG505 DS-SOSIP



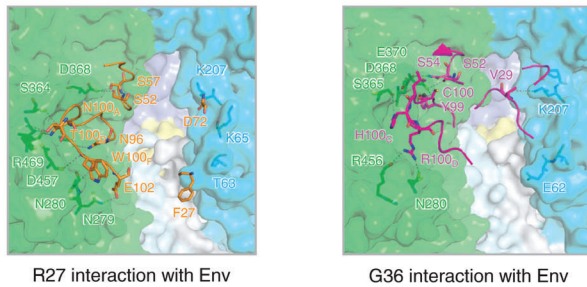
C Comparison of epitopes of R27, G36 and J3



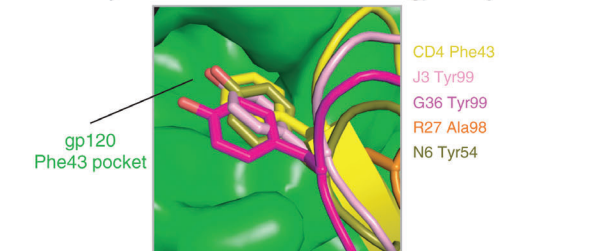
D Comparison of binding modes and angles



E Interaction of nanobodies with HIV-1 Env



G Mimicry of CD4 Phe43 interaction with gp120 by nanobodies



F Nanobody sequences and paratope residues

	1	22	31	36	50	66	82ABC	92	95	100	103	111
HV3S61*01	QVQLVESGGGLVQPGGSLRLS	CAASGFTLDYIAIGWFRQAPGKERE	GVSCISSD	SGSTYYADSVKGRFTISRDN	AKNTVYLQMN	SLKPEGTAVVY	C					
R25	QVQLQESGGGLVQPGGSLRLS	CAAS EDSL EDYIAIGWFRQAPGK HE GVAC ITGS VGNTHYAD FV EGRFTISR	DDKNTVY	LEMNSLKPE DTAL YYCAIQRF	GCA NR WTFYV DS MKGKQT	VTVSS						
R27	QVQLQESGGGLVQPGGSLRLS	CAVSG ED ENYSIGWFRQAPG KA EGVAC LKNS G IG ---	SVKGRFTISR	GDS NT WFL QMG AL E AD TAVYTCATY NR ACAN Y V T I W ---	FRGGQT	VTVSS						
G36	QVQLQESGGGLVQPGGSLRLS	CAVSG GLD V ES VTIGWFRQAPG KE RE EV GC IS GN FD Q TY VDSV	KGRFTISR	VNE ENTVYLQ MD N L K P ED TAT YYCV T D R Q F Y CA L H R L P V S Q YR	GGQT	VTVSS						
HV3-3*01	QVQLVESGGGLVQAGGSLRLS	CAASGRTPSSYAMGFRQAPGKEREF	VAAISWSGGSTYYADSVKGRFTISR	DNKNTVYLQMN	SLKPEDTAVVY	CA						
J3	EV QLV ES GGGLVQAG GFL EL SC EL GS IF EG YAMWFRQAPGKEREF	VAG MD LP YGE ---	FVKGRFTISR	DA K ST VYLQ MS LE PD T AI Y FC ARS GS Y Q Y R GG Q T V T V SS								

Figure 4. Cryo-EM structures of nanobodies R27 and G36 in complex with HIV-1 Env trimer reveal modes of recognition similar to J3. A) Cryo-EM structure of nanobody R27 in complex with HIV-1 BG505 DS-SOSIP Env. Overall cryo-EM density map and refined model are shown in two views with gp120 protomers colored green, cyan, and slate, respectively. The density and model of nanobody R27 is colored orange. The contour level of Cryo-EM map is 9.5 σ . B) Cryo-EM structure of VHH G36 in complex with HIV-1 BG505 DS-SOSIP Env. Overall cryo-EM density map and refined model are shown in two views with gp120 protomers colored green, cyan, and slate, respectively. The density and model of G36 is colored magenta. The contour level of Cryo-EM map is 9.6 σ . C) Epitopes of R27 and G36 on BG505 DS-SOSIP. Epitopes of R27, G36, and J3 are shown in orange, magenta, and pink surfaces, respectively. R27 has a much smaller contact area on the neighboring protomer. D) Comparison of binding modes and angles. (Left) Structures of nanobodies R27, G36, and J3 are aligned with CD4 by the gp120 domain shown in green. R27, G36, and J3 are roughly in a similar position with N

2.6. Ultrapotent and Broad HIV-1 Neutralizing Bispecific Antibodies

To further improve the potency and breadth, we attached the two CD4bs-targeting nanobodies, G36 and R27, to the N-terminus of the light chain of a V2-apex-targeting broadly neutralizing antibody CAP256V2LS^[22] (Figure 5A), creating human-llama bispecific antibodies.^[6] A 38-strain panel test showed that conjugating nanobody monomers (G36, R27, and J3) with CAP256V2LS improved neutralization potency over their triplet conjugation on human IgG1 Fc domain (x3-IgG2a format described above) (Figure 5B). While CAP256L-G36×3LS was not better than CAP256L-G36LS, both CAP256L-R27×3LS and CAP256L-J3×3LS substantially improved neutralizing potency, with CAP256L-R27×3LS being the most potent (geometric mean IC₅₀ = 0.004 μg mL⁻¹). We then tested CAP256L-G36×3LS and CAP256L-R27×3LS on an additional 42 strains. Data obtained from an overall 80-strain panel showed that the two bispecific antibodies neutralized over 94% of cross-clade HIV-1 viruses ultrapotently, with geometric mean IC₅₀s of 0.012 and 0.003 μg mL⁻¹, respectively (Figure 5C, with explicit IC₅₀ and IC₈₀ values provided in Dataset S1, Supporting Information). Even though we did not test them on a larger panel, the 80-strain panel data allowed us to make reliable estimations of the breadth and potency of the two bispecific antibodies on 208-strain panel (Figure S9, Supporting Information).^[23] The estimated neutralization IC₈₀ on a 208-strain panel suggested the combined potency and breadth for CAP256L-R27×3 to exceed other published HIV-1 bNAbS, as well as previously reported multi-specific antibodies (Figure 5D, with predicted IC₅₀ and IC₈₀ values provided in Dataset S1, Supporting Information).

2.7. Structural Basis for the Broad HIV-1 Neutralization of CAP256L-R27×3LS

We were unable to obtain a cryo-EM structure for CAP256L-R27×3 bound to BG505 DS-SOSIP due to antibody-induced aggregation but did succeed in determining a cryo-EM structure for CAP256L-R27 bound to BG505 DS-SOSIP. This structure revealed a single CAP256V2LS Fab to bind at the V2-apex and three copies of R27 each to bind to a CD4bs of the trimer (Figure 6; Figure S10, Table S1, Supporting Information). Even though the cryo-EM density for the linker between R27 and CAP256 light chain was disordered, one of the bound R27s could be identified by its proximity to link with the light chain of CAP256 that bound to the V2-apex (Figure 6), and the other two R27s were from separate CAP256L-R27 molecules (Figure S10F, Supporting Information).

2.8. Autoreactivity and Enhanced Pharmacokinetics of CAP256L-R27×3LS

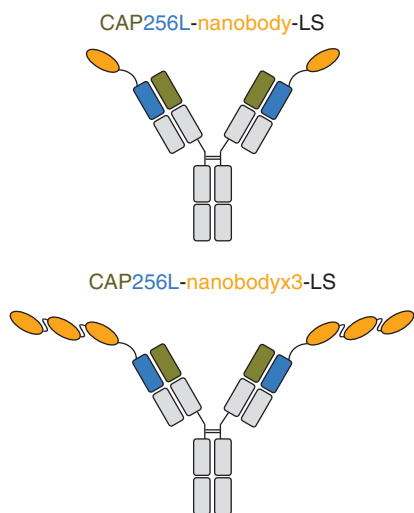
Finally, to evaluate whether the newly identified and engineered R27-related nanobody molecules are suitable for clinical use, we sought to determine their autoreactivity and pharmacokinetics. While three control antibodies, 4E10, VRC07-523LS, and VRC07-G54W, showed binding scores of 1, 2, and 3, respectively, neither R27 nor its variants showed binding to Hep-2 cells, indicating no antinuclear antibody (ANA) response (Figure 7A). R27, R27-IgG2a, and R27×3-IgG2a showed no binding to cardiolipin. Only CAP256L-R27LS and CAP256L-R27×3LS showed low levels of binding to cardiolipin, which is similar to that of CAP256.J3LS (Figure 7B). Depending on administration methods, nanobody x3 was reported to have a very short half-life in mice, ranging from 0.8 to 9.5 hours.^[24] Our pharmacokinetics analysis using human FcRn-Fc-KI mice revealed that although Fc conjugation can extend the half-life of G36×3 and R27×3, they were cleared from mice within 5 days (Figure 7C). While monomeric R27 conjugated to CAP256 exhibited a bit longer but still less than optimal half-life, the CAP256L-R27×3LS half-life was just a little bit shorter than the parent CAP256V2LS (Figure 7C).

3. Discussion

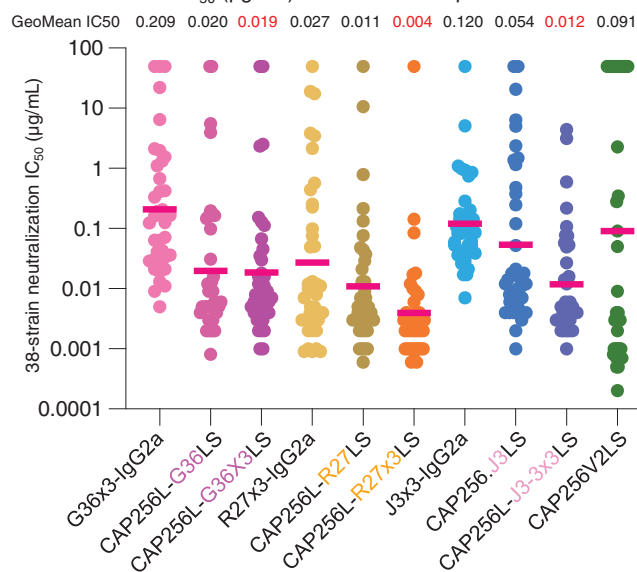
Multiple animal species have evolved alternatives to the heavy-light antibody recognition utilized by the human immune system,^[5,18,25] and these alternatives provide unique ways to bypass HIV's Env defenses. Immunization in cows with prefusion-closed Env trimer elicits broadly neutralizing antibodies, with cow-specific D-regions of up to 48 residues, extending from the body of the antibody to reach conserved elements of the CD4bs.^[25a] Immunization in llamas with gp140 elicited nanobodies such as J3, with VHH recognition enabled mimicry of CD4.^[5,19] Serum neutralization however from the gp140 immunized llamas was not broadly neutralizing. Here we show how immunizations of a llama with a prefusion-closed trimer initially yielded only autologous neutralization, but after repeated immunizations developed a broadly neutralizing response. Three doses of immunization with the same immunogen in humans yield autologous neutralizing antibodies that target the fusion-peptide site of vulnerability.^[10,11] Short-term immunization of BG505 DS-SOSIP seems to direct most of the antibody response to the glycan-free base region, partially due to the inaccessibility of broadly neutralizing epitopes covered by surface glycans. It is possible that initially elicited, base-targeting non-neutralizing antibodies cover the highly immunogenic glycan-free base, allowing antibody responses against neutralizing epitopes to develop after extended periods of immunizations. Indeed, broad serum neutralization responses were observed after 6 times of BG505

termini (labeled with "N") in close proximity. (Right) The axes of R27, G36, and J3 are shown in orange, magenta, and pink rods. Axes of CD4 domain 1 and Fv domain of VRC01-class antibody N6 are shown in yellow and olive rods for comparison. E) Detailed interactions between nanobodies and BG505 DS-SOSIP. Residues that form hydrogen bonds and salt bridges are highlighted with sticks representation with bonds between atoms shown in gray dotted lines. Nanobodies and protomers of HIV Env are colored the same as in panels A and B. F) Alignment of nanobody sequences. Paratope residues are colored in orange and magenta, respectively. Residues interacting with neighboring protomer are colored in lighter shades. Residues interacting with both protomers are underlined. G) Nanobody mimicry of CD4 Phe43 interaction with gp120. G36, like J3, inserts Tyr99 into the "Phe43 pocket" on gp120, whereas R27 has an Ala at this position.

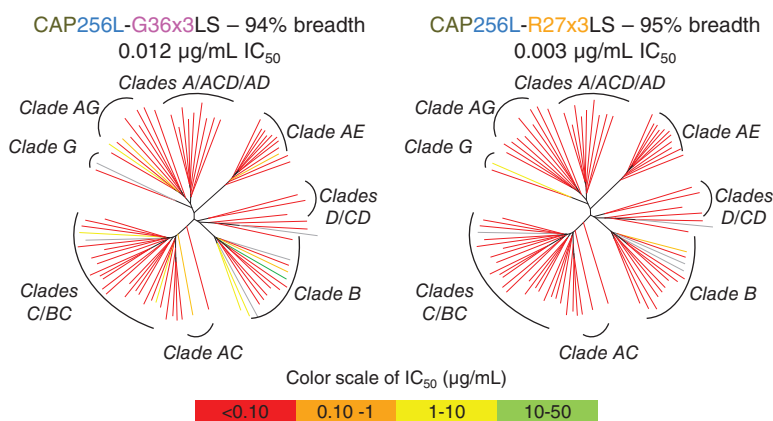
A Schematic of CAP256L-nanobody chimera



B Neutralization IC₅₀ (μg/mL) on the 38-strain panel



C 80-strain neutralization (IC₅₀)



D Human-llama bispecific versus other antibodies

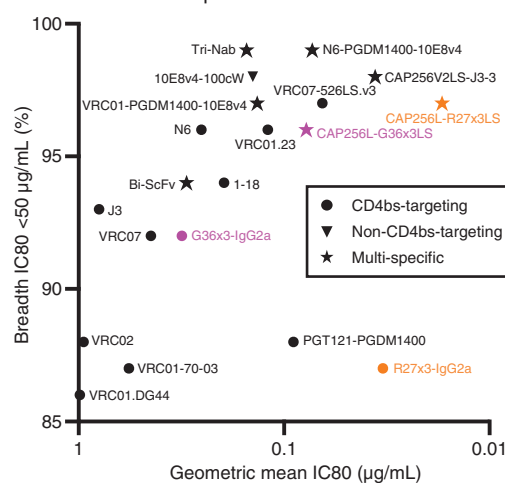


Figure 5. Ultra-potent HIV-1 bispecific antibodies from attaching nanobodies to the light chain of V2-apex-directed antibody CAP256V2LS. A) Schematic of CAP256L-nanobody chimeras. B) 38-strain neutralization of nanobodies. C) 80-strain panel neutralization. Dendrograms display the diversity of tested viral strains, with branches colored according to neutralization potency (non-neutralized branches shown in gray). D) Comparison of neutralization breadth and potency for R27 and G36 constructs with other potent antibodies on the 208-strain panel. Data for CAP256L-G36x3LS and CAP256L-R27x3LS are estimated from 80-strain data in panel C. Bispecific and trispecific antibodies are shown as stars.

DS-SOSIP immunization, which was still improving in terms of both breadth and potency when we terminated the study on day 271. More importantly, although the CD4bs may have been difficult to access due to their surrounding glycans, the elicited serum neutralization was mapped to be primarily VRC01-like, and therefore CD4bs targeting.

We further identified CD4bs nanobodies with substantially higher potency than J3. While nanobody phage library screening using glycan base-covered trimer only identified two neutralizing nanobodies, G36 and Day271_G1, screening with CD4bs-specific subdomain probe RSC3 led to many neutralizing nanobodies exclusively targeting the CD4bs. CDR comparison and lineage analysis allowed us to identify nanobody candidates of interest from day 271 library based on neutralizing data of the nanobodies in

the same lineage from the day 188 library. Although G36 and R27 both recognize CD4bs on HIV-1 Env trimer, they demonstrated highly differential neutralization potency and breadth. The triplicate format (nanobody x3-IgG2a) resulted in more potency improvement for R27 than for G36, which is likely due to their different binding pattern and approaching angles to the CD4bs. It is worth noting that the enhanced potency was not proportional to the number of CD4bs-binding moieties in these molecules, suggesting a complex mechanism of neutralization. A combination of G36, R27, or J3, especially their triplicate format with the potent V2-directed antibody, CAP256V2LS, yielded bispecifics with even greater neutralization potency.

Nanobody multimerization followed by bispecific conjugation with compatible human antibodies seems to be a generalizable

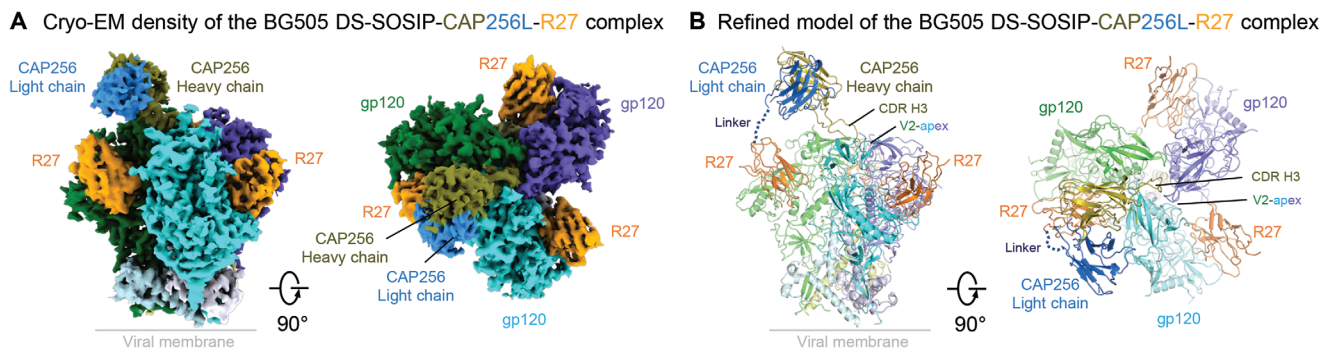


Figure 6. Cryo-EM structure of CAP256L-R27LS Fab in complex with HIV-1 Env reveals CAP256 and R27 to bind prefusion-closed trimer at V2-apex and CD4bs simultaneously. Cryo-EM density A) and refined model B) for the CAP256-R27-BG505 DS SOSIP complex were shown in two 90°-views and colored by chains. The chimera antibody bound to the HIV-1 Env with CAP256L CDR H3 (colored olive) inserted into the V2-apex and the CAP256L light chain (skyblue)-linked R27 contacting one of the CD4-binding sites, however, the density of the flexible linker between R27 and CAP256L light chain was disordered. Three copies of R27 were observed to bind to each of the 3 CD4bs on the HIV-1 Env trimer, indicating the other two R27s were from different chimeric antibodies.

strategy for nanobody function improvement. Of note, the newly engineered CAP256L-J3-3×3LS, a human-llama bispecific antibody conjugating the triplicate of J3 variants J3-3 to CAP256V2LS, exhibited more than 4 times improved potency than the previously reported bispecific antibody CAP256.J3LS. The best of the bispecifics from this study, CAP256L-R27×3LS, was three times more potent than CAP256L-J3-3×3LS and reached levels of potency that rivaled the previously reported best multi-specific antibodies developed thus far. CAP256L-R27×3LS neutralized 93% of an 80-strain panel with a geometric mean IC_{80} of $0.008 \mu\text{g mL}^{-1}$. Computational extrapolation predicted neutralization of the 208-strain panel with a breadth of 97% and a geometric mean IC_{80} of $0.017 \mu\text{g mL}^{-1}$ (Figure S9A, Supporting Information). In comparison, the previously reported bispecific antibody with the best potency, CAP256V2LS-J3-3, neutralizes 98% of the 208-strain panel with a geometric mean IC_{80} of $0.036 \mu\text{g mL}^{-1}$,^[6] and trispecific antibody N6-PGDM1400-10E8v4 neutralizes 99% with a geometric mean IC_{80} of $0.073 \mu\text{g mL}^{-1}$.^[7] We note that if VRC01 had comparable potency as CAP256L-R27×3LS, the prevention efficacy would be expected to exceed 90% in the antibody-mediated prevention (AMP) study.^[26]

It is believed that low-dose repeated mucosal challenge in macaques closely mimics clinical HIV-1 infection scenarios.^[27] In one such study, a single injection of 10–1074, 3BNC117, or VRC01 protected macaques from SHIV_{AD8} infection until the median plasma concentrations declined to $0.17 - 1.83 \mu\text{g mL}^{-1}$, values that are comparable to their IC_{80} s determined in vitro.^[28] If the observed correlation between virus breakthrough and in vitro IC_{80} s of bNAbs holds true for different virus strains in humans, given its extremely low IC_{80} , the protective serum level of CAP256L-R27×3LS in humans could be at least 500-fold below $10 \mu\text{g mL}^{-1}$. Importantly, CAP256L-R27×3LS is not auto-reactive at such a low concentration in our assay. Although CAP256L-R27×3LS exhibited a slightly shorter half-life than CAP256V2LS alone, its superior potency and breadth make it a promising bNAb for therapeutic and/or prophylactic application. Additional strategies such as reduction of net positive charge^[29] or through FC alterations, such asYTE (M252Y/S254I/T256E)^[30] or DHS (L309D/Q311H/N434S),^[31] may enable its half-life to be further extended.

It remains to be seen if this bispecific can avoid anti-antibody responses to enable its therapeutic and prophylactic use in humans. When used as an HIV-1 therapeutic, the simultaneous targeting of V2-apex and CD4bs on HIV-1 Env trimers by CAP256L-R27×3LS will likely result in less viral escape. In the future, it would also be interesting to see whether the glycan-base-covered BG505 DS-SOSIP^[32] or combinations of heterologous base-covered Env trimers can elicit broader neutralizing responses with less immunizations or over a shorter time period.

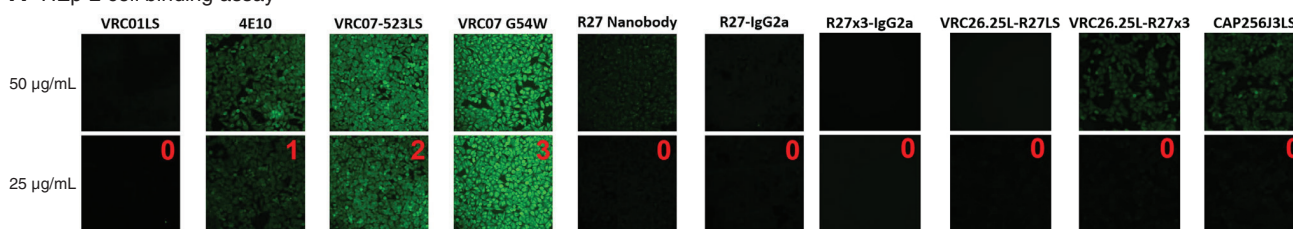
4. Experimental Section

Expression and Purification of BG505 DS-SOSIP and Related Proteins: BG505 DS-SOSIP protein was expressed and purified as previously described.^[9] Glycan-base (BG505 DS-SOSIP.4mut_N502-660) and CD4bs knockout (KO 4115) constructs of BG505 were expressed with an N-terminal scFc tag, separated by an HRV-3C cleavage site. The plasmids were transfected into Freestyle 293-F cells (Thermo) and protein was expressed for 6 days at 37 °C. The cell supernatant was collected by centrifugation and applied to Protein A resin (Cytiva), after which the HIV Env was liberated by cleavage with HRV-3C. The flowthrough was collected and applied to a Superdex S-200 gel filtration column, after which the protein was concentrated to 1 mg mL^{-1} , flash frozen with 10% glycerol, and stored at $-80 \text{ }^\circ\text{C}$ until use. His-tagged RSC3 was first purified from day-5 supernatant of transiently transfected 293F cells using Ni-NTA-resin (Qiagen) and monomeric RSC3 was further purified through a HiLoad 16/600 Superdex200 sizing column (Cytiva) on an AKTA Pure FPLC system. HIV-1 fusion peptide (FP8) was synthesized and biotinylated by GenScript.

Llama Immunizations and Nanobody Phage Library Construction: Llama immunization procedures were performed by following Capralogics Inc. ACUC protocol. One llama (Capralogics) was immunized subcutaneously with 1 mg of recombinant BG505 DS-SOSIP protein in the presence of Complete Freund's Adjuvant (CFA) at day 0, and boost immunized with 0.5 mg of BG505 DS-SOSIP protein in the presence of Incomplete Freund's Adjuvant (IFA) on day 21, 42, 63, 84, 105, 126, 147, 168, 189, 210, 231, and 257, respectively. Test blood/serum samples were taken on days 0, 52, 73, 94, 115, 136, 157, 178, 199, 220, 241, and 271 for antibody-antigen binding tests and neutralization tests. 300 mL of whole blood were collected on days 188 and 271, and peripheral blood mononuclear cells (PBMCs) were isolated and used for nanobody phage library construction as previously described.^[18]

Phage Screening for HIV-1 Env Binding Nanobodies: Four HIV-1 Env-related proteins were used for phage screening: Env trimer (BG505

A HEP-2 cell binding assay



B Summary of autoreactivity

Antibodies	HEP-2 score	GPL unit			
		100 µg/mL	33.3 µg/mL	11.1 µg/mL	3.7 µg/mL
VRC01LS	0	3.88	1.91	1.88	2.29
4E10	1	219.08	217.51	214.10	197.02
VRC07-523LS	2	32.13	12.84	4.24	2.45
VRC07-523 G54W	3	101.29	34.92	15.98	5.61
R27 nanobody	0	2.27	1.47	1.75	1.93
R27-IgG2a	0	2.84	2.02	2.32	2.06
R27x3-IgG2a	0	1.82	2.07	1.62	1.87
CAP256L-R27LS	0	77.06	30.79	10.83	3.73
CAP256L-R27x3LS	0	86.47	38.82	13.80	5.63
CAP256.J3LS	0	50.98	18.04	7.56	3.70

<15	Negative	20-80	Low to medium positive
15-20	Indeterminate	>80	High positive

C Half-life

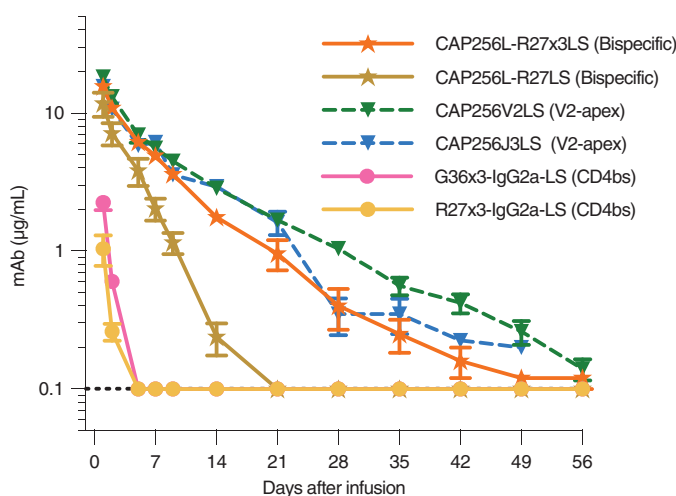


Figure 7. CAP256L-R27x3LS autoreactivity and half-life in human FcRn-Fc KI mice. A) Autoreactivity of antibodies determined by HEP-2 cell binding assay. B) Summary of autoreactivity of antibodies determined by HEP-2 cell binding assay and anti-cardiolipin ELISA assay. C) In vivo half-life of CAP256L-nanobody variants assessed in a human FcRn-Fc knock-in mouse model.

DS-SOSIP), Glycan base trimer (BG505 DS-SOSIP.4mut_N502-660), RSC3 and biotinylated Fusion peptide. For Env trimer, glycan base trimer or RSC3 screening, three wells of MaxiSorp 96-well plate (Thermo Fisher Scientific) were first coated with lectin (EMD Millipore, L8275, 100 µg mL⁻¹ in PBS) at 4 °C overnight, washed with PBS with 0.1% Tween-20 three times and blocked with 5% non-fat milk in PBS at room temperature for 1 h, then coated with 50 µL of 100 µg mL⁻¹ proteins at room temperature for 2 h. One well without target protein was included as a non-coated control. For biotinylated FP8 screening, two wells of Streptavidin-coated plate (Thermo Fisher Scientific) were coated with 50 µL of FP8 (100 µg mL⁻¹ in PBS) at 4 °C overnight, washed and blocked with non-fat milk. Another well with 50 µL of PBS was used as a non-coated control. Nanobody phages were added to wells and screened as previously described.^[18]

Enzyme-Linked Immunosorbent Assay: After one or two rounds of selection, TG-1 cells from sub-libraries were plated and colonies were picked to prepare periplasmic extracts containing crude nanobodies. Serum samples from different time points and nanobody candidates were tested for their binding to individual target proteins by enzyme-linked immunosorbent assay (ELISA) as previously described.^[18] In brief, glycan proteins were coated onto Maxisorp plates indirectly through lectin, and biotinylated FP8 was coated to streptavidin-coated plates. Plates were washed and blocked, and then 100 µL of diluted serum samples or undiluted nanobody-containing supernatant were added and incubated for 2 h at room temperature. Horseradish peroxidase (HRP) conjugated goat anti-alpaca VHH domain-specific antibody (Jackson ImmunoResearch) and tetramethylbenzidine (TMB) (Thermo Fisher Scientific) were used for de-

veloping ELISA signals, which were measured with Synergy microplate reader (BioTek Gen5).

Expression and Purification of Nanobodies and Fc Conjugated Nanobody Variants: Nanobodies were expressed and purified as previously described.^[18] In brief, phagemids of lead nanobodies were extracted from TG-1 cells and transformed into WK6 cells (ATCC). WK6 cells were cultured in 2YT medium and induced by IPTG for nanobody expression. Cells were pelleted and treated with polymyxin B to release nanobodies from periplasmic region. Nanobodies in the supernatant were purified using a Capturem His-tagged purification kit (Takara) or complete His-tag purification resin (Roche), dialyzed, and filtered sterile before being used for downstream assays. Monomeric or multimeric nanobody sequences were fused to the Fc region of human IgG1 through llama IgG2a hinge and cloned into the pVRC8400 vector. In multimeric form, nanobody units were connected through (GGGGG)₃ flexible linkers. The Fc fusion constructs were expressed in Expi293 cells and antibodies in the supernatant were purified using protein A, concentrated, dialyzed, and filtered sterile.

HIV Neutralization: Neutralization was measured using single-round-of-infection HIV-1 Env-pseudoviruses and TZM-bl target cells, as described previously.^[33] Neutralization curves were fit by nonlinear regression using a 5-parameter hill slope equation. The neutralization titers were calculated as a reduction in luminescence units compared with control wells and reported as 50% or 80% inhibitory concentration (IC₅₀ or IC₈₀) in micrograms per milliliter.

Biolayer Interferometry Assay for Epitope Mapping: A 96-Channel Ultra High Throughput Octet RH96 System was used to map the binding

epitopes of 6xHis-tagged nanobodies. Assays were performed at 30 °C in tilted black 384-well plates (Geiger Bio-One) in PBS + 0.02% Tween20, 0.1% BSA, 0.05% sodium azide with agitation set to 1000 rpm. His-tagged nanobodies (50 $\mu\text{g mL}^{-1}$) were loaded onto Ni-NTA biosensors for 150 seconds. Bindings to HIV-1 Env were measured by dipping immobilized nanobodies into solutions of 200 nM BG505 DS-SOSIP without or with 720 nM Fabs of antibodies with known epitopes for 180 seconds. Fabs of antibodies VRC01, VRC34.01, 1E6, PGT145 and 10–1074 were used for competing the CD4bs, FP, Env-base, V2-apex and glycan V3 epitopes, respectively. Parallel correction to subtract systematic baseline drift was carried out by subtracting the measurements recorded for a loaded sensor dipped into a buffer-only control well. The degree of competition was calculated as (the ratio of responses between BG505 DS-SOSIP in the presence of blocking Fab and BG505 DS-SOSIP alone) $\times 100\%$ and defined as three categories: complete (<30%), partial (30–60%) and slight (60–80%).

Biolayer Interferometry Assay to Measure Nanobody Affinity: The BLI assay was performed using a Sartorius Octet R2 instrument to determine the affinity of BG505 DS-SOSIP to nanobodies. In brief, 6xHis-tagged G36 and R27 were immobilized onto Ni-NTA biosensors at 10 $\mu\text{g mL}^{-1}$, and G36x3-IgG2a and R27x3-IgG2 were immobilized onto Protein A biosensors at 20 $\mu\text{g mL}^{-1}$ for 60 seconds. Biosensors were then dipped into a solution containing BG505 DS-SOSIP for 300 seconds followed by dissociation for 600 seconds. Sensorgrams of the concentration series were corrected with corresponding blank curves and fitted globally with Octet evaluation software using a 1:2 bivalent analyte model of binding.

Cryo-EM Data Collection, Processing, and Model Refinement: Cryo-EM specimens of HIV-1 Env trimer BG505 DS-SOSIP complexes with nanobodies R27 and G36 were prepared by vitrification using a ThermoFisher Scientific Vitrobot Mark IV plunger. Quantifoil R 2/2 gold grids were glow-discharged using a PELCO easiGlow glow-discharger (air pressure: 0.39 mBar, current: 20 mA, duration: 30 s) immediately before use. Data was collected using SerialEM^[34] with a ThermoFisher Titan Krios G1 electron microscope equipped with a Gatan K2 Summit direct electron detector operating in the counting mode (Table S1, Supporting Information). For structure of CAP256L-R27LS Fab in complex with BG505 DS-SOSIP, Env was mixed with the CAP256L-R27LS Fab at 1.0 to 1.2 molar ratio (protomer to Fab) at a final total protein concentration of $\approx 3\text{--}4\text{ mg mL}^{-1}$ and adjusted to have a final concentration of 0.005% (w/v) n-Dodecyl β -D-maltoside (DDM) to prevent preferred orientation and aggregation during vitrification. Cryo-EM grids were prepared by applying 3 μL of sample to a fresh glow-discharged carbon-coated copper grid (CF 1.2/1.3 300 mesh). The sample was vitrified in liquid ethane using a Vitrobot Mark IV with a wait time of 30 s, a blot time of 3 s, and a blot force of 0. Cryo-EM data were collected on a Titan Krios operating at 300 keV, equipped with a K3 detector (Gatan) operating in counting mode. Data were acquired using Legion.^[35] The dose was fractionated over 50 raw frames.

Cryo-EM data process workflow for the BG505 DS-SOSIP in complex with llama nanobodies and the bi-specific antibody, including motion correction, CTF estimation, particle picking and extraction, 2D classification, ab initio reconstruction, heterogeneous refinement, homogeneous refinement, non-uniform refinement, and local resolution estimation, were carried out in cryoSPARC 3.3.^[36] For the three complexes, 315969, 414002, and 236154 particles, respectively, were selected after 3D Ab-Initio classification and heterogeneous refinement for further refinement, and final cryo-EM density maps after sequential homogeneous and non-uniform refinements were used for iterative manual model building and real-space refinement in Coot^[37] and in Phenix.^[38] The coordinates of cryo-EM structures J3-BG505 DS-SOSIP (PDB ID: 7LPN) and CAP256V2LS-J3-3-BG505 DS-SOSIP (PDB ID: 8FIS) were used as initial models. Molprobity^[39] was used to validate geometry and check structure quality at each iteration step. UCSF Chimera and ChimeraX^[40] were used for map fitting and manipulation.

Antibody-Env interface Analysis: The buried interface areas, hydrogen bonds, and salt bridges between the bound antibodies and HIV-1 Env were analyzed using the PDBePISA website (<https://www.ebi.ac.uk/pdbe/pisa/pistart.html>).^[41]

Neutralization Fingerprint Analysis: The neutralization fingerprints of day 188 and day 271 serum samples, defined as the potency pattern with

which the sera neutralized a set of 60 HIV-1 strains, were analyzed and compared as described previously.^[14]

Nanobody Lineage Analysis: Nucleotide sequences were submitted to IMGT Vquest server to assign the germline gene (https://www.imgt.org/IMGT_vquest/input). The phylogenetic trees were prepared by gctree with default parameters.^[42]

Pharmacokinetic Study in Human Neonatal Fc receptor-Fc (FcRn-Fc) Transgenic Mice: Human FcRn-Fc transgenic mice (FcRn-/- hFcRn-Fc Tg mice, JAX stock # 029686, The Jackson Laboratory) were used to assess the pharmacokinetics of selected antibodies. Each animal was infused intravenously with 5 mg mAb/kg of body weight. Whole blood samples were collected on days 1, 2, 5, 7, 9, 14, 21, 28, 35, 42, 49, and 56. Serum mAb levels were measured by ELISA using an anti-idiotypic antibody to CAP256 or BG505 DS-SOSIP trimer as described previously.^[43] All mice were bred and maintained under pathogen-free conditions at the American Association for the Accreditation of Laboratory Animal Care-accredited Animal Facility at the National Institute of Allergy and Infectious Diseases and housed in accordance with the procedures outlined in the Guide for the Care and Use of Laboratory Animals. All the mice were between 6 and 13 weeks of age. The study protocol was evaluated and approved by the National Institutes of Health's Animal Care and Use Committee (ASP VRC-20-893).

Predicting Nanobody Neutralization Against 208 HIV-1 Isolates: Using the measured neutralization for bispecific antibodies against 80 HIV-1 isolates, it was extrapolated how these antibodies-of-interest would neutralize a larger panel of 208 isolates. Briefly, the measurements were combined with neutralization from 80 reference monoclonal antibodies measured against the 208 isolates. Then matrix completion was applied via nuclear norm minimization, which found linear combinations of the reference antibodies that matched the neutralization from the antibodies of interest and used these linear combinations to infer the remaining measurements.^[23] To assess prediction error, 10% of available measurements and applied matrix completion were withheld to compare the predicted-versus-measured values. The error of these predictions was 4-fold (i.e., a predicted $\text{IC}_{80} = 0.4\text{ }\mu\text{g mL}^{-1}$ should lie between $0.4/4 = 0.1$ and $0.4 \times 4 = 1.6\text{ }\mu\text{g mL}^{-1}$), far smaller than 10^7 -fold range of the neutralization data. As done previously, IC_{80} s were inverted and logged ($\text{IC}_{80} \rightarrow \log_{10}[1/\text{IC}_{80}]$) prior to matrix completion and then reverted after matrix completion.^[23] Inverting ensures that the smallest values representing the strongest responses were predicted more accurately than weak responses. Log transformation prevents strong neutralization measurements from overpowering the predictions. Each reference antibody had at least 40 concrete measurements against the 80-isolate panel (i.e., ignoring bounded values such as $\text{IC}_{80} > 100\text{ }\mu\text{g mL}^{-1}$) to enable comparison with the antibodies of interest. For each antibody of interest, the fraction of the 208-isolate panel was isolated which it neutralized with an $\text{IC}_{80} < 50\text{ }\mu\text{g mL}^{-1}$. To account for the 4-fold prediction error, several thousand simulations were run, where every predicted IC_{80} was multiplied by a factor between $1/4$ and 4 (equally sampled in a log-scale), the number of IC_{80} s $< 50\text{ }\mu\text{g mL}^{-1}$ was counted, and fit the resulting distribution.

Autoreactivity: The autoreactivity of the antibodies was assessed using the ANA Hep-2 Test System (ZEUS Scientific, Cat. No: FA2400EB) and anticardiolipin ELISA kit (Inova Diagnostics Cat. No.: 708625). Briefly, to evaluate the binding of the antibodies to Hep-2 cells, all the antibodies were tested at 25 and 50 $\mu\text{g mL}^{-1}$ in PBS buffer following the instructions from the manufacturer of the ANA Hep-2 Test System. The VRC01LS, 4E10, VRC07-523-LS, and VRC07-G54W antibodies were used as controls. Slides were imaged on a Nikon Eclipse Ts2R microscope with a 20x objective lens for 500 ms. The fluorescent signals of the control antibodies at 25 $\mu\text{g mL}^{-1}$ were scored as 0, 1, 2, and 3, respectively. The fluorescent signals of the test antibodies were estimated visually in comparison to the control ones. Scores over 1 at 25 $\mu\text{g mL}^{-1}$ were defined as autoreactive and between 0 and 1 as mildly autoreactive. For the cardiolipin ELISA, all the antibodies were tested at 100 $\mu\text{g mL}^{-1}$, followed by a 3-fold serial dilution. IgG phospholipid (GPL) units were derived from the standard curve. A GPL score below 20 was considered as not reactive, between 20 and 80 as a low positive, and greater than 80 as a high positive. The reported results were representative of two independent experiments.

Data Presentation: Figures were arranged in PowerPoint.

Statistical Analysis: Statistical analysis was performed with GraphPad Prism 9 software. Neutralization titers of individual strains were calculated by fitting nonlinear regression using a five-parameter hill slope equation, and the panels IC₅₀ and IC₈₀ were presented as geometric mean. The exact sample size for each experimental group was reported in figure legend and/or shown in figure as the number of branches or dots. The *p*-value < 0.05 was considered to be significant.

Supporting Information

Supporting Information is available from the Wiley Online Library or from the author.

Acknowledgements

The authors thank J. Stuckey for assistance with figures and members of the Virological Laboratory, Vaccine Research Center for comments and discussions. The author also thank R. Carroll, N. Jean-Baptiste, K. McKee, C. Moore, S. O'Dell, S.D., Schmidt, C. Whittaker, and A.B. McDermott for their assistance with neutralization assessments on the 208-strain panel, J.R. Mascola for advice and support on antibody neutralization assays, and J. Baalwa, D. Ellenberger, F. Gao, B. Hahn, K. Hong, J. Kim, F. McCutchan, D. Montefiori, L. Morris, E. Sanders-Buell, G. Shaw, R. Swanstrom, M. Thomson, S. Tovanabutra, C. Williamson, and L. Zhang for contributing the HIV-1 envelope plasmids used in the neutralization panel. The authors thank the VRC Production Program for providing BG505 DS-SOSIP. The authors also thank the Columbia University Cryo-Electron Microscopy Center for cryo-EM data collection for the complex structure of CAP256L-R27LS Fab with BG505 DS-SOSIP. Funding was provided by the Vaccine Research Center, an intramural Division of the National Institute of Allergy and Infectious Diseases (NIAID), NIH, ZIA AI005022, by the Intramural Research Program of the Office of AIDS Research, NIAID, NIH, 1ZIAAR999999-01 and by the Intramural Research Program of the Division of Intramural Research, National Institute of Arthritis and Musculoskeletal and Skin Diseases, NIH. This work was funded in part by the Frederick National Laboratory for Cancer Research, NIH, under contract HHSN261200800001, and by federal funds from the National Cancer Institute, NIH, under contract no. 75N910D00024. This work was also supported in part by the Georgia State University startup funding (to J.X.).

Conflict of Interest

The National Institutes of Health was in the process of filing a patent application in connection with this work on which J.X., T.Z., B.Z., A.F.N., A.P., C.S., Y.D.K, A.S.O., E.S.Y., N.A.D., R. Casellas, and P.D.K. were contributors. Other authors declare no competing interests.

Author Contributions

J.X. and T.Z. contributed equally to this work. J.X., T.Z., R. Casellas, and P.D.K. conceptualized the project. J.X. led the llama immunization, nanobody identification, production, and engineering studies. T.Z. led the epitope mapping and cryo-EM studies. K.M., S.O., and E.T. performed neutralization analysis. B.Z. engineered and produced bispecific antibodies. C.L. and J.M. performed autoreactivity analysis. A.F.N. performed epitope mapping analysis. A.P. led the pharmacokinetic analysis. C.S. performed nanobody lineage analysis. M.F.B. and Y.D.K. produced antibodies for pharmacokinetic analysis. A.C., R. Chaudhary, X.C., A.S.O., and I-T.T. provided critical reagents. T.E. performed the 208-strain neutralization estimation analysis. B.C.L. and M.K.L. performed a 208-strain neutralization analysis. J.E.B., N.C.M., R.S.R., and T.S. collected cryo-EM data. R.R. performed a neutralization fingerprinting analysis. P.C. produced nanobodies and performed kinetics analysis. S.W. assisted with data visualization.

E.S.Y. performed the pharmacokinetic analysis. Y.T., L.S. led the cryo-EM data collection. N.A.D. led the neutralization analysis. J.X., T.Z., S.W., and P.D.K. wrote the original draft of the paper, and all authors reviewed and approved the final manuscript.

Data Availability Statement

The data that support the findings of this study are openly available in the Electron Microscopy Data Bank and Protein Data Bank under entry IDs EMD-41415, EMD-41416, EMD-41417, and PDB IDs 8TNG, 8TNH, 8TNI, respectively.

Keywords

bispecific antibodies, bNAb, broadly neutralizing antibody, HIV-1, llama, neutralizing nanobodies, vaccination, vaccine

Received: November 29, 2023

Revised: March 22, 2024

Published online:

- [1] C. Hamers-Casterman, T. Atarhouch, S. Muyldermans, G. Robinson, C. Hamers, E. B. Songa, N. Bendahman, R. Hamers, *Nature* **1993**, 363, 446.
- [2] S. Muyldermans, *Annu. Rev. Biochem.* **2013**, 82, 775.
- [3] a) N. A. Doria-Rose, J. N. Bhiman, R. S. Roark, C. A. Schramm, J. Gorman, G. Y. Chuang, M. Pancera, E. M. Cale, M. J. Erndes, M. K. Louder, M. Asokan, R. T. Bailer, A. Druz, I. R. Fraschilla, N. J. Garrett, M. Jarosinski, R. M. Lynch, K. McKee, S. O'Dell, A. Pegu, S. D. Schmidt, R. P. Staupe, M. S. Sutton, K. Wang, C. K. Wibmer, B. F. Haynes, S. Abdool-Karim, L. Shapiro, P. D. Kwong, P. L. Moore, et al., *J. Virol.* **2016**, 90, 76; b) J. Gorman, G. Y. Chuang, Y. T. Lai, C. H. Shen, J. C. Boyington, A. Druz, H. Geng, M. K. Louder, K. McKee, R. Rawi, R. Verardi, Y. Yang, B. Zhang, N. A. Doria-Rose, B. Lin, P. L. Moore, L. Morris, L. Shapiro, J. R. Mascola, P. D. Kwong, *Cell Rep.* **2020**, 31, 107488; c) N. A. Doria-Rose, C. A. Schramm, J. Gorman, P. L. Moore, J. N. Bhiman, B. J. DeKosky, M. J. Erndes, I. S. Georgiev, H. J. Kim, M. Pancera, R. P. Staupe, H. R. Altae-Tran, R. T. Bailer, E. T. Crooks, A. Cupo, A. Druz, N. J. Garrett, K. H. Hoi, R. Kong, M. K. Louder, N. S. Longo, K. McKee, M. Nonyane, S. O'Dell, R. S. Roark, R. S. Rudicell, S. D. Schmidt, D. J. Sheward, C. Soto, et al., *Nature* **2014**, 509, 55; d) J. Huang, B. H. Kang, E. Ishida, T. Zhou, T. Griesman, Z. Sheng, F. Wu, N. A. Doria-Rose, B. Zhang, K. McKee, S. O'Dell, G. Y. Chuang, A. Druz, I. S. Georgiev, C. A. Schramm, A. Zheng, M. G. Joyce, M. Asokan, A. Ransier, S. Darko, S. A. Migueles, R. T. Bailer, M. K. Louder, S. M. Alam, R. Parks, G. Kelsoe, T. Von Holle, B. F. Haynes, D. C. Douek, et al., *Immunity* **2016**, 45, 1108; e) R. Kong, K. Xu, T. Zhou, P. Acharya, T. Lemmin, K. Liu, G. Ozorowski, C. Soto, J. D. Taft, R. T. Bailer, E. M. Cale, L. Chen, C. W. Choi, G. Y. Chuang, N. A. Doria-Rose, A. Druz, I. S. Georgiev, J. Gorman, J. Huang, M. G. Joyce, M. K. Louder, X. Ma, K. McKee, S. O'Dell, M. Pancera, Y. Yang, S. C. Blanchard, W. Mothes, et al., *Science* **2016**, 352, 828; f) R. Pejchal, K. J. Doores, L. M. Walker, R. Khayat, P. S. Huang, S. K. Wang, R. L. Stanfield, J. P. Julien, A. Ramos, M. Crispin, R. Depetris, U. Katpally, A. Marozsan, A. Cupo, S. Malveste, Y. Liu, R. McBride, Y. Ito, R. W. Sanders, C. Ogohara, J. C. Paulson, T. Feizi, C. N. Scanlan, C. H. Wong, J. P. Moore, W. C. Olson, A. B. Ward, P. Poignard, W. R. Schief, D. R. Burton, et al., *Science* **2011**, 334, 1097; g) P. Schommers, H. Gruell, M. E. Abernathy, M. K. Tran, A. S. Dingens, H. B. Gristick, C. O. Barnes, T. Schoofs, M. Schlotz, K. Vanshylla, C. Kreer, D. Weiland, U. Holtick, C. Scheid, M. M. Valter, M. J. van Gils, R. W. Sanders,

- J. J. Vehreschild, O. A. Cornely, C. Lehmann, G. Fatkenheuer, M. S. Seaman, J. D. Bloom, P. J. Bjorkman, F. Klein, *Cell* **2020**, *180*, 471; h) D. Sok, M. J. van Gils, M. Pauthner, J. P. Julien, K. L. Saye-Francisco, J. Hsueh, B. Briney, J. H. Lee, K. M. Le, P. S. Lee, Y. Hua, M. S. Seaman, J. P. Moore, A. B. Ward, I. A. Wilson, R. W. Sanders, D. R. Burton, *Proc Natl Acad Sci U S A* **2014**, *111*, 17624; i) X. Wu, Z. Y. Yang, Y. Li, C. M. Hogerkorp, W. R. Schief, M. S. Seaman, T. Zhou, S. D. Schmidt, L. Wu, L. Xu, N. S. Longo, K. McKee, S. O'Dell, M. K. Louder, D. L. Wycuff, Y. Feng, M. Nason, N. Doria-Rose, M. Connors, P. D. Kwong, M. Roederer, R. T. Wyatt, G. J. Nabel, J. R. Mascola, *Science* **2010**, *329*, 856.
- [4] a) P. Hraber, M. S. Seaman, R. T. Bailer, J. R. Mascola, D. C. Montefiori, B. T. Korber, *AIDS* **2014**, *28*, 163; b) M. D. Simek, W. Rida, F. H. Priddy, P. Pung, E. Carrow, D. S. Laufer, J. K. Lehrman, M. Boaz, T. Tarragona-Fiol, G. Miiro, J. Birungi, A. Pozniak, D. A. McPhee, O. Manigart, E. Karita, A. Inwoley, W. Jaoko, J. Dehovitz, L. G. Bekker, P. Pitisuttithum, R. Paris, L. M. Walker, P. Poignard, T. Wrin, P. E. Fast, D. R. Burton, W. C. Koff, *J. Virol.* **2009**, *83*, 7337; c) X. Wu, Z. Zhang, C. A. Schramm, M. G. Joyce, Y. D. Kwon, T. Zhou, Z. Sheng, B. Zhang, S. O'Dell, K. McKee, I. S. Georgiev, G. Y. Chuang, N. S. Longo, R. M. Lynch, K. O. Saunders, C. Soto, S. Srivatsan, Y. Yang, R. T. Bailer, M. K. Louder, N. C. S. Program, J. C. Mullikin, M. Connors, P. D. Kwong, J. R. Mascola, L. Shapiro, *Cell* **2015**, *161*, 470.
- [5] L. E. McCoy, A. F. Quigley, N. M. Strokappe, B. Bulmer-Thomas, M. S. Seaman, D. Mortier, L. Rutten, N. Chander, C. J. Edwards, R. Ketteler, D. Davis, T. Verrips, R. A. Weiss, *J. Exp. Med.* **2012**, *209*, 1091.
- [6] B. Zhang, J. Gorman, Y. D. Kwon, A. Pegu, C. W. Chao, T. Liu, M. Asokan, M. F. Bender, T. Bylund, L. Damron, D. Gollapudi, P. Lei, Y. Li, C. Liu, M. K. Louder, K. McKee, A. S. O'Neil, R. Rawi, A. Schon, S. Wang, E. S. Yang, Y. Yang, K. Carlton, N. A. Doria-Rose, L. Shapiro, M. S. Seaman, J. R. Mascola, P. D. Kwong, *mAbs* **2023**, *15*, 2165390.
- [7] L. Xu, A. Pegu, E. Rao, N. Doria-Rose, J. Beninga, K. McKee, D. M. Lord, R. R. Wei, G. Deng, M. Louder, S. D. Schmidt, Z. Mankoff, L. Wu, M. Asokan, C. Beil, C. Lange, W. D. Leuschner, J. Kruip, R. Sendak, Y. D. Kwon, T. Zhou, X. Chen, R. T. Bailer, K. Wang, M. Choe, L. J. Tartaglia, D. H. Barouch, S. O'Dell, J. P. Todd, D. R. Burton, et al., *Science* **2017**, *358*, 85.
- [8] J. J. Steinhart, J. Guenaga, H. L. Turner, K. McKee, M. K. Louder, S. O'Dell, C. I. Chiang, L. Lei, A. Galkin, A. K. Andrianov, A. D.-R. N., R. T. Bailer, A. B. Ward, J. R. Mascola, Y. Li, *Nat. Commun.* **2018**, *9*, 877.
- [9] Y. D. Kwon, M. Pancera, P. Acharya, I. S. Georgiev, E. T. Crooks, J. Gorman, M. G. Joyce, M. Guttman, X. Ma, S. Narpala, C. Soto, D. S. Terry, Y. Yang, T. Zhou, G. Ahlsen, R. T. Bailer, M. Chambers, G. Y. Chuang, N. A. Doria-Rose, A. Druz, M. A. Hallen, A. Harned, T. Kirys, M. K. Louder, S. O'Dell, G. Ofek, K. Osawa, M. Prabhakaran, M. Sastry, G. B. Stewart-Jones, et al., *Nat. Struct. Mol. Biol.* **2015**, *22*, 522.
- [10] K. V. Houser, M. R. Gaudinski, M. Happe, S. Narpala, R. Verardi, E. K. Sarfo, A. R. Corrigan, R. Wu, R. S. Rothwell, L. Novik, C. S. Hendel, I. J. Gordon, N. M. Berkowitz, C. T. Cartagena, A. T. Widge, E. E. Coates, L. Strom, S. Hickman, M. Conan-Cibotti, S. Vazquez, O. Trofymenko, S. Plummer, J. Stein, C. L. Case, M. Nason, A. Biju, D. K. Parchment, A. Changela, C. Cheng, et al., *EClinicalMedicine* **2022**, *48*, 101477.
- [11] S. Wang, F. Matassoli, B. Zhang, T. Liu, C. H. Shen, T. Bylund, T. Johnston, A. R. Henry, I. T. Teng, P. Tripathi, J. E. Becker, A. Changela, R. Chaudhary, C. Cheng, M. Gaudinski, J. Gorman, D. R. Harris, M. Lee, N. C. Morano, L. Novik, S. O'Dell, A. S. O'Neil, D. K. Parchment, R. Rawi, J. Roberts-Torres, T. Stephens, Y. Tsybovsky, D. Wang, D. J. Van Wazer, T. Zhou, et al., *Cell Rep.* **2023**, *42*, 112755.
- [12] K. Xu, P. Acharya, R. Kong, C. Cheng, G. Y. Chuang, K. Liu, M. K. Louder, S. O'Dell, R. Rawi, M. Sastry, C. H. Shen, B. Zhang, T. Zhou, M. Asokan, R. T. Bailer, M. Chambers, X. Chen, C. W. Choi, V. P. Dandey, N. A. Doria-Rose, A. Druz, E. T. Eng, S. K. Farney, K. E. Foulds, H. Geng, I. S. Georgiev, J. Gorman, K. R. Hill, et al., *Nat. Med.* **2018**, *24*, 857.
- [13] N. A. Doria-Rose, H. R. Altae-Tran, R. S. Roark, S. D. Schmidt, M. S. Sutton, M. K. Louder, G. Y. Chuang, R. T. Bailer, V. Cortez, R. Kong, K. McKee, S. O'Dell, F. Wang, S. S. Abdool Karim, J. M. Binley, M. Connors, B. F. Haynes, M. A. Martin, D. C. Montefiori, L. Morris, J. Overbaugh, P. D. Kwong, J. R. Mascola, I. S. Georgiev, *PLoS Pathog.* **2017**, *13*, e1006148.
- [14] I. S. Georgiev, N. A. Doria-Rose, T. Zhou, Y. D. Kwon, R. P. Staupe, S. Moquin, G. Y. Chuang, M. K. Louder, S. D. Schmidt, H. R. Altae-Tran, R. T. Bailer, K. McKee, M. Nason, S. O'Dell, G. Ofek, M. Pancera, S. Srivatsan, L. Shapiro, M. Connors, S. A. Migueles, L. Morris, Y. Nishimura, M. A. Martin, J. R. Mascola, P. D. Kwong, *Science* **2013**, *340*, 751.
- [15] C. A. Cottrell, J. van Schooten, C. A. Bowman, M. Yuan, D. Oyen, M. Shin, R. Morpurgo, P. van der Woude, M. van Breemen, J. L. Torres, R. Patel, J. Gross, L. M. Sewall, J. Copps, G. Ozorowski, B. Nogal, D. Sok, E. G. Rakasz, C. Labranche, V. Vigdorovich, S. Christley, D. G. Carnathan, D. N. Sather, D. Montefiori, G. Silvestri, D. R. Burton, J. P. Moore, I. A. Wilson, R. W. Sanders, A. B. Ward, et al., *PLoS Pathog.* **2020**, *16*, e1008753.
- [16] J. H. Lee, R. Andrabi, C. Y. Su, A. Yasmeen, J. P. Julien, L. Kong, N. C. Wu, R. McBride, D. Sok, M. Pauthner, C. A. Cottrell, T. Nieuwsma, C. Blattner, J. C. Paulson, P. J. Klasse, I. A. Wilson, D. R. Burton, A. B. Ward, *Immunity* **2017**, *46*, 690.
- [17] H. Mouquet, L. Scharf, Z. Euler, Y. Liu, C. Eden, J. F. Scheid, A. Halper-Stromberg, P. N. Gnanapragasam, D. I. Spencer, M. S. Seaman, H. Schuitemaker, T. Feizi, M. C. Nussenzweig, P. J. Bjorkman, *Proc Natl Acad Sci U.S.A.* **2012**, *109*, E3268.
- [18] J. Xu, K. Xu, S. Jung, A. Conte, J. Lieberman, F. Muecksch, J. C. C. Lorenzi, S. Park, F. Schmidt, Z. Wang, Y. Huang, Y. Luo, M. S. Nair, P. Wang, J. E. Schulz, L. Tessarollo, T. Bylund, G. Y. Chuang, A. S. O'Neil, T. Stephens, I. T. Teng, Y. Tsybovsky, T. Zhou, V. Munster, D. D. Ho, T. Hatzioannou, P. D. Bieniasz, M. C. Nussenzweig, P. D. Kwong, R. Casellas, *Nature* **2021**, *595*, 278.
- [19] T. Zhou, L. Chen, J. Gorman, S. Wang, Y. D. Kwon, B. C. Lin, M. K. Louder, R. Rawi, E. D. Stancovski, Y. Yang, B. Zhang, A. F. Quigley, L. E. McCoy, L. Rutten, T. Verrips, R. A. Weiss, V. R. C. P. Program, N. A. Doria-Rose, L. Shapiro, P. D. Kwong, *Structure* **2022**, *30*, 862.
- [20] T. Zhou, I. Georgiev, X. Wu, Z. Y. Yang, K. Dai, A. Finzi, Y. Do Kwon, J. Scheid, W. Shi, L. Xu, Y. Yang, J. Zhu, M. C. Nussenzweig, J. Sodroski, L. Shapiro, G. J. Nabel, J. R. Mascola, P. D. Kwong, *Science* **2010**, *329*, 811.
- [21] T. Zhou, J. Zhu, X. Wu, S. Moquin, B. Zhang, P. Acharya, I. S. Georgiev, H. R. Altae-Tran, G. Y. Chuang, M. G. Joyce, Y. D. Kwon, N. S. Longo, M. K. Louder, T. Luongo, K. McKee, C. A. Schramm, J. Skinner, Y. Yang, Z. Yang, Z. Zhang, A. Zheng, M. Bonsignori, B. F. Haynes, J. F. Scheid, M. C. Nussenzweig, M. Simek, D. R. Burton, W. C. Koff, N. C. S. Program, J. C. Mullikin, et al., *Immunity* **2013**, *39*, 245.
- [22] B. Zhang, D. Gollapudi, J. Gorman, S. O'Dell, L. F. Damron, K. McKee, M. Asokan, E. S. Yang, A. Pegu, B. C. Lin, C. W. Chao, X. Chen, L. Gama, V. B. Ivleva, W. H. Law, C. Liu, M. K. Louder, S. D. Schmidt, C. H. Shen, W. Shi, J. A. Stein, M. S. Seaman, A. B. McDermott, K. Carlton, J. R. Mascola, P. D. Kwong, Q. P. Lei, N. A. Doria-Rose, *Sci. Rep.* **2022**, *12*, 17876.
- [23] T. Einav, B. Cleary, *Cell Syst* **2022**, *13*, 561.
- [24] X. Wu, L. Cheng, M. Fu, B. Huang, L. Zhu, S. Xu, H. Shi, D. Zhang, H. Yuan, W. Nawaz, P. Yang, Q. Hu, Y. Liu, Z. Wu, *Cell Rep.* **2021**, *37*, 109869.
- [25] a) D. Sok, K. M. Le, M. Vadnais, K. L. Saye-Francisco, J. G. Jardine, J. L. Torres, Z. T. Berndsen, L. Kong, R. Stanfield, J. Ruiz, A. Ramos, C. H. Liang, P. L. Chen, M. F. Criscitiello, W. Mwangi, I. A. Wilson, A. B. Ward, V. V. Smider, D. R. Burton, *Nature* **2017**, *548*, 108; b) R. A. Weiss, C. T. Verrips, *Vaccines (Basel)* **2019**, *7*, 77.

- [26] a) L. Corey, P. B. Gilbert, M. Juraska, D. C. Montefiori, L. Morris, S. T. Karuna, S. Edupuganti, N. M. Mgodhi, A. C. deCamp, E. Rudnicki, Y. Huang, P. Gonzales, R. Cabello, C. Orrell, J. R. Lama, F. Laher, E. M. Lazarus, J. Sanchez, I. Frank, J. Hinojosa, M. E. Sobieszczyk, K. E. Marshall, P. G. Mukwekwerere, J. Makhema, L. R. Baden, J. I. Mullins, C. Williamson, J. Hural, M. J. McElrath, C. Bentley, et al., *N. Engl. J. Med.* **2021**, *384*, 1003; b) N. N. Mkhize, A. E. J. Yssel, H. Kaldine, R. T. van Dorsten, A. S. Woodward Davis, N. Beaume, D. Matten, B. Lambson, T. Modise, P. Kgagudi, T. York, D. H. Westfall, E. E. Giorgi, B. Korber, C. Anthony, R. E. Mapengo, V. Bekker, E. Domin, A. Eaton, W. Deng, A. DeCamp, Y. Huang, P. B. Gilbert, A. Gwashu-Nyangiwe, R. Thebus, N. Ndabambi, D. Mielke, N. Mgodhi, S. Karuna, S. Edupuganti, et al., *PLoS Pathog.* **2023**, *19*, 1011469; c) K. E. Seaton, Y. Huang, S. Karuna, J. R. Heptinstall, C. Brackett, K. Chiong, L. Zhang, N. L. Yates, M. Sampson, E. Rudnicki, M. Juraska, A. C. deCamp, P. T. Edlefsen, J. I. Mullins, C. Williamson, R. Rossen Khan, E. E. Giorgi, A. Kenny, H. Angier, A. Randhawa, J. A. Weiner, M. Rojas, M. Sarzotti-Kelsoe, L. Zhang, S. Sawant, M. E. Ackerman, A. B. McDermott, J. R. Mascola, J. Hural, M. J. McElrath, et al., *EBioMedicine* **2023**, *93*, 104590.
- [27] H. Gruell, F. Klein, *Retrovirology* **2018**, *15*, 73.
- [28] R. Gautam, Y. Nishimura, A. Pegu, M. C. Nason, F. Klein, A. Gazumyan, J. Golijanin, A. Buckler-White, R. Sadjadpour, K. Wang, Z. Mankoff, S. D. Schmidt, J. D. Lifson, J. R. Mascola, M. C. Nussenzweig, M. A. Martin, *Nature* **2016**, *533*, 105.
- [29] Y. D. Kwon, A. Pegu, E. S. Yang, B. Zhang, M. F. Bender, M. Asokan, Q. Liu, K. McKee, B. C. Lin, T. Liu, M. K. Louder, R. Rawi, M. Reveiz, A. J. Schaub, C. H. Shen, N. A. Doria-Rose, P. Lusso, J. R. Mascola, P. D. Kwong, *mAbs* **2023**, *15*, 2223350.
- [30] W. F. Dall'Acqua, R. M. Woods, E. S. Ward, S. R. Palaszynski, N. K. Patel, Y. A. Brewah, H. Wu, P. A. Kiener, S. Langermann, *J. Immunol.* **2002**, *169*, 5171.
- [31] C. H. Lee, T. H. Kang, O. Godon, M. Watanabe, G. Delidakis, C. M. Gillis, D. Sterlin, D. Hardy, M. Cogne, L. E. Macdonald, A. J. Murphy, N. Tu, J. Lee, J. R. McDaniel, E. Makowski, P. M. Tessier, A. S. Meyer, P. Bruhns, G. Georgiou, *Nat. Commun.* **2019**, *10*, 5031.
- [32] A. S. Olia, C. Cheng, T. Zhou, A. Biju, D. R. Harris, A. Changela, H. Duan, V. B. Ivleva, W. P. Kong, L. Ou, R. Rawi, Y. Tsybovsky, D. J. Van Wazer, A. R. Corrigan, C. A. Gonelli, M. Lee, K. McKee, S. Narpala, S. O'Dell, D. K. Parchment, E. D. Stancofski, T. Stephens, I. Tan, I. T. Teng, S. Wang, Q. Wei, Y. Yang, Z. Yang, B. Zhang, V. R. C. P. Program, et al., *iScience* **2023**, *26*, 107403.
- [33] M. Sarzotti-Kelsoe, R. T. Bailer, E. Turk, C. L. Lin, M. Bilska, K. M. Greene, H. Gao, C. A. Todd, D. A. Ozaki, M. S. Seaman, J. R. Mascola, D. C. Montefiori, *J. Immunol. Methods* **2014**, *409*, 131.
- [34] D. N. Mastronarde, *J. Struct. Biol.* **2005**, *152*, 36.
- [35] A. Cheng, C. Negro, J. F. Bruhn, W. J. Rice, S. Dallakyan, E. T. Eng, D. G. Waterman, C. S. Potter, B. Carragher, *Protein Sci.* **2021**, *30*, 136.
- [36] A. Punjani, J. L. Rubinstein, D. J. Fleet, M. A. Brubaker, *Nat. Methods* **2017**, *14*, 290.
- [37] P. Emsley, K. Cowtan, *Acta Crystallogr D Biol Crystallogr* **2004**, *60*, 2126.
- [38] P. D. Adams, P. V. Afonine, G. Bunkoczi, V. B. Chen, I. W. Davis, N. Echols, J. J. Headd, L. W. Hung, G. J. Kapral, R. W. Grosse-Kunstleve, A. J. McCoy, N. W. Moriarty, R. Oeffner, R. J. Read, D. C. Richardson, J. S. Richardson, T. C. Terwilliger, P. H. Zwart, *Acta Crystallogr D Biol Crystallogr* **2010**, *66*, 213.
- [39] C. J. Williams, J. J. Headd, N. W. Moriarty, M. G. Prisant, L. L. Videau, L. N. Deis, V. Verma, D. A. Keedy, B. J. Hintze, V. B. Chen, S. Jain, S. M. Lewis, W. B. Arendall 3rd., J. Snoeyink, P. D. Adams, S. C. Lovell, J. S. Richardson, D. C. Richardson, *Protein Sci* **2018**, *27*, 293.
- [40] E. F. Pettersen, T. D. Goddard, C. C. Huang, G. S. Couch, D. M. Greenblatt, E. C. Meng, T. E. Ferrin, *J Comput Chem* **2004**, *25*, 1605.
- [41] E. Krissinel, K. Henrick, *J Mol Biol* **2007**, *372*, 774.
- [42] W. S. DeWitt, L. Mesin, G. D. Victora, V. N. Minin, F. A. t. Matsen, *Mol Biol Evol* **2018**, *35*, 1253.
- [43] R. S. Rudicell, Y. D. Kwon, S. Y. Ko, A. Pegu, M. K. Louder, I. S. Georgiev, X. Wu, J. Zhu, J. C. Boyington, X. Chen, W. Shi, Z. Y. Yang, N. A. Doria-Rose, K. McKee, S. O'Dell, S. D. Schmidt, G. Y. Chuang, A. Druz, C. Soto, Y. Yang, B. Zhang, T. Zhou, J. P. Todd, K. E. Lloyd, J. Eudailey, K. E. Roberts, B. R. Donald, R. T. Bailer, J. Ledgerwood, N. C. S. Program, et al., *J Virol* **2014**, *88*, 12669.